

UNIVERSITY OF TWENTE

FACULTY OF ENGINEERING TECHNOLOGY
LABORATORY OF THERMAL ENGINEERING

Master's Thesis

Determining design relations for a magnetocaloric device with multiple magneto caloric materials using numerical software.

Author

C.P.J. Ridderhof

Supervisors

prof.dr.ir. Th.H. van der Meer

dr.ir. G.G.M. Stoffels

dr.ir. Mina Shahi

Exam committee

prof.dr.ir. Th.H. van der Meer

prof.dr.ir. M. ter Brake

dr.ir. G.G.M. Stoffels

dr.ir. Mina Shahi

May 7, 2017

PREFACE

With the health of the earthly environment high on the public agenda, conventional heating and cooling techniques are in need of replacing due to efficiency and environmental reasons. Active heat transfer will be done differently, more eco-friendly, in the near future. The magnetocaloric effect may be at the foundation of a new heat pump. In order to create an economical feasible heat pump significant improvements have to be made concerning the total heat transfer coefficient.

This thesis represents the work I did as my master assignment for the department of mechanical engineering, at the faculty of thermodynamic engineering at the Twente University. The main purpose of my assignment was to further investigate the magneto caloric effect and develop a 2D model of the AMR. This model was already initiated by Jöran Stoter a previous master student. The model needed further improvements and validation. Next to this the use of a different materials has been implemented. Materials developed by the department of material sciences of TU Delft have been used.

I would like to express my sincere gratitude to my supervisors: professor van der Meer and doctor Stoffels. I always felt motivated to continue to work on the thesis. I hope this work provides a contribution to the research of eco-friendly heat pumps,

Joost Ridderhof

May 7, 2017

SUMMARY

This thesis describes the research into the magneto caloric effect(MCE) and the use of it in a regenerative setting, or active magneto regenerator(AMR). The MCE is first described with thermodynamics. From previous research at the Twente University it seems that the energy balance as found in the thermodynamics does not hold up. The thermodynamics found are tested in a 0D-model. This means only the temporal domain will be used. The thermodynamics are implemented into a model in Matlab. When using a small enough time-step the energy balance does hold up. It can be concluded that the thermodynamics are validated. In order to describe the MCE the material properties are of great importance. They are described with the use of the 'Mean Field Theory'(MFT).

In the second part of the thesis a 2D model of an AMR is created with gadolinium as magneto caloric material (MCM). This model is made with the software program Comsol Multi-physics. At first a mesh study is performed looking for an optimal spatial and temporal resolution where the computational time is kept at reasonable lengths. In order to prove that the model is representative, two validation methods are used. At first a quasi analytical solution is used to validate the cooling capacity. This also provides for feedback concerning the energy balance. The second validation uses data as found in literature. The model is given the same dimensions as provided by literature. The model provides the same behaviour at various utilization factors as found in literature. However the magnitude varies greatly: the model does not include a heat-loss model apparently.

To engineer a heat pump capable of handling larger temperature differences other MCM is required than gadolinium. The third part of this thesis describes the numerical research into the so-called Brück materials named after one of the founding fathers of this material. This material can be used as MCM due to its giant magneto caloric effect whilst retaining optimal material properties such as minimal hysteresis or physical deformations. The Curie temperature of this material can be changed by altering the composition. The literature describes various material families and for this thesis the $Mn_{1.25}Fe_{0.7}P_{1-y}Si_y$ family is used, where $y = 0.49, 0.50, 0.51$ or 0.52 . The Curie temperatures are from lower to higher values respectively. The new 2D-model describes these material as placed next to each other in successive Curie temperature. The material properties are derived from literature.

Looking at the derived material properties from this literature it seems that the adiabatic temperature change differs from the calculated temperature change. This difference is accounted for by the presence of latent heat, which is not described by the thermodynamics of the MCE. This latent heat due to the transition in magnetic state of the material: from ferromagnetic to paramagnetic. In order to account for the extra heat produced the internal magnetization derivative is amplified slightly. Observing the properties further reveals a heat capacity that changes varies greatly due to the applied magnetic field. This raises the hypothesis that this material will perform better in a heating set-up instead of a cooling set-up. In order to validate this a study is conducted where the utilization factor is plotted against the obtained temperature span. This study is done twofold: first with a constant temperature cold heat exchanger, second with a constant temperature hot heat exchanger. It seems that the first set-up obtains a larger temperature difference with respect with the second set-up. During the experiments the temperature gradient varies greatly with a greatly varying heat capacity as a consequence, the result is a non-functional utilization factor. The most important recommendation therefore is to perform an experiment where the fluid displacement distance is varied, based upon an expected heat capacity whilst retaining a constant utilization factor for each thermodynamic cycle.

SAMENVATTING

Deze thesis beschrijft het onderzoek naar het magneto calorisch effect en het gebruik ervan in een regeneratieve opstelling ook wel actief magnetische regenerator (AMR) genoemd. Hiertoe wordt eerst het magneto calorisch effect beschreven in een thermodynamische afleiding. In vorige onderzoeken aan de Twente University blijkt dat de energiebalans niet intact is. Hiertoe wordt de beschreven thermodynamische afleiding getoetst in een 0D-setting. Dat wil zeggen dat er gebruik gemaakt wordt van een domein in de temporele ruimte. Het model is geïmplementeerd in Matlab en het blijkt dat bij een afdoende kleine tijdstap alle beschreven energieën elkaar opheffen en daardoor kan geconcludeerd worden dat de thermodynamica gevalideerd blijkt. Om het magneto calorische effect te beschrijven zijn de materiaaleigenschappen van belang. De materiaaleigenschappen van gadolinium worden beschreven door de zogenaamde 'Mean Field Theory'.

In het tweede deel wordt een 2D model van een AMR beschreven. Dit model is gemaakt in het softwarepakket COMSOL. Als eerste wordt er gekeken welke spatiele en temporele resoluties stabiele resultaten geven. Het blijkt dat binnen acceptabele rekentijden stabiele resultaten kunnen worden gehaald. Om het model van enige zingeving te voorzien wordt een quasi analytische afleiding gedaan van het magneto calorische effect, waarna wordt gekeken of het model dezelfde uitkomst geeft. Om het model verder te valideren wordt gebruik gemaakt van in literatuur gevonden karakteristieken. De dimensionalisering wordt gedaan aan de hand van in dezelfde literatuur beschreven experimenten. Het blijkt dit 2D model hetzelfde gedrag beschrijft als gevonden in literatuur. Eén verschil is overduidelijk aanwezig: het model omvat geen geïmplementeerd warmte-verlies-model.

Om een warmtepomp te maken die een groter temperatuurbereik aan kan moet er gekeken worden naar andere materialen dan gadolinium. Het derde deel van deze master thesis beschrijft het numerieke onderzoek naar een zogenaamd Brück materiaal in een 2D model. Deze naam is afgeleid naar de naam van de onderzoeksgroep leider: prof. Brück. Dit materiaal verdient de aandacht omdat het materiaal een groot magneto calorisch effect ondergaat bij het opleggen van een magneetveld. Daarbij kan het materiaal worden aangepast om bij de heersende temperaturen een groot MCE te laten zien. De literatuur beschrijft verschillende materiaal families die dergelijke effecten laten zien, voor deze thesis wordt gebruik gemaakt van de $Mn_{1.25}Fe_{0.7}P_{1-y}Si_y$ familie, waar $y = 0.49, 0.50, 0.51$ of 0.52 kan zijn. De Curie temperaturen volgen elkaar respectievelijk op. Het volgende 2D model omvat deze materialen naast elkaar geplaatst in opvolgende Curie temperatuur. De materiaaleigenschappen zijn afgeleid uit de literatuur. Uit de gevonden materiaaleigenschappen blijkt dat het magneto calorische effect de warmte die vrijkomt als gevonden in de literatuur niet beschrijft. Er blijkt sprake te zijn van zogenaamde latente warmte die vrijkomt bij de overgang van de ferromagnetische toestand naar de paramagnetische. Om dit verschil op te vangen wordt de afgeleide van de interne magnetisatie curve versterkt. Verder blijkt dat door een asymmetrie in de warmtecapaciteit dat het materiaal zich beter leent in een opstelling waar een koude warmtebron is opgesteld tegen over een warm koellichaam. Om dit aan te tonen wordt een studie gedaan naar de maximale temperatuur spanne bij verschillende utilisatie factoren. Deze studie wordt tweemaal gedaan. In eerste instantie wordt de koude warmtewisselaar op constante temperatuur gehouden en in de tweede wordt de warme warmtewisselaar op constante temperatuur gehouden. Het blijkt met de koude warmtewisselaar op constante temperatuur een groter temperatuurspanne kan worden opgebouwd in vergelijking met de warme warmtewisselaar.

De belangrijkste aanbeveling naar aanleiding van de numerieke experimenten is om de vloeistofslag voor elke magneto calorische cyclus te variëren op basis van de verwachte gemiddelde warmtecapaciteit voor die cyclus ten einde de utilisatie factor gelijk te houden gedurende het experiment.

CONTENTS

Preface	i
Summary	iii
Samenvatting	v
1 Introduction	1
1.1 Heat pumps	1
1.2 The magnetocaloric effect	1
1.3 Active Magnetic Regenerator	2
2 Fundamentals of the magnetocaloric effect	5
2.1 Introduction	5
2.2 Energy	5
2.2.1 Isothermal entropy change	6
2.2.2 Adiabatic temperature change	7
2.3 Cyclic operation	8
3 Material properties	9
3.1 Transition Temperature T_C	9
3.1.1 1 st and 2 nd order transitions	9
3.2 Material properties of Gadolinium	9
3.3 The Weiss Mean Field Model	10
3.4 The Debye & Sommerfeld model	11
3.5 Theoretical material properties	11
3.5.1 Heat Capacity	11
3.5.2 Magnetization	11
3.5.3 Temperature derivative of magnetization with respect to temperature	12
3.6 Material Properties of $Mn_{1.25}Fe_{0.7}P_{1-y}Si_y$	13
3.6.1 Heat capacity	13
3.6.2 Magnetization	16
3.6.3 Density and thermal conductivity	17
4 0D-Model	19
4.1 Model set up	19
4.1.1 Numerical Implementation	19
4.1.2 Modelling the magnetic field	20
4.2 Results and Discussion	22
4.2.1 Temporal Study	23
4.2.2 Discussion	24

5 Active magnetic Regenerator	25
5.1 2D model - Gadolinium	25
5.2 Model Design	27
5.2.1 The convective Term	28
5.2.2 Input parameters	28
5.2.3 Mesh and Time stepping	29
5.3 Validation	31
5.4 Results	32
5.5 Discussion	32
6 2D model - $Mn_{1.25}Fe_{0.7}P_{1-y}Si_y$ -AMR	35
6.1 Introduction	35
6.2 Experiments	36
6.3 Results	37
6.3.1 0D Temperature experiments	37
6.3.2 2D Utilization experiments	38
6.4 discussion	42
7 Conclusion and Discussion	43
7.1 0D model	43
7.2 2D model - Gadolinium	43
7.3 2D model - $Mn_{1.25}Fe_{0.7}P_{1-y}Si_y$	43
7.3.1 Recommendation: 2.5D model	44
7.3.2 Recommendation: Utilization factor	44
Bibliography	I
Nomenclature	III
0D model figures	V
Full Results 2D model	VII

INTRODUCTION

1.1 HEAT PUMPS

The current focus upon the human effect on climate change requires a more efficient way of heat transport. Climates where both heating and cooling are required, the heat pump offers an energy-efficient way of replacing furnaces or air-conditioners. The magnetocaloric heat pump requires electricity to move heat from a cold source towards a hot sink: the refrigerator cycle. Moving heat against the temperature gradient is the soulpurpose of a heat pump.

Currently the most used heat pump relies on the vapor-compression cycle. The heat is being moved using a closed-loop cycle: compressing, condensing, expanding and evaporating a refrigerant fluid. The configuration of the system will determine whether the net effect is the cooling or heating of a specified volume. There are various reasons why this type of heat pump is dominant: it is scalable, relatively compact, has a high reliability and efficient operation at 30 to 60 % of Carnot. This system can be found in AC-units in cars or refrigerators at home.

Most of these system use fluids, called refrigerants, are harmful for the environment. Due to the great number of moving parts in such a system the durability is affected. Next to this, due to moving parts, the system can be very loud. The last reason being the relative low efficiency in comparison to promising magnetocaloric heat pumps [1] [2], [3]. Due to an increasing cooling/heating demand the impact of these systems on the energy consumption is high [4]. Therefor by investigating alternative heat-pumps the human effect on climate change could be altered in a positive way [5].

1.2 THE MAGNETOCALORIC EFFECT

Magnetocaloric energy conversion is a technique based upon the use of the magnetocaloric effect, or MCE for short. The occurrence of the MCE happens under the influence of a changing applied magnetic field on a ferromagnetic material[6].

Two distinctive cases are usually described concerning the way the MCE is described: adiabatic or isothermally. In isothermal conditions the temperature is kept constant at all times whether in adiabatic conditions there is no heat transfer from or to the domain (magnetocaloric material). In the last case a temperature difference could be measured, whereas the isothermal case describes how much energy is being transferred to or from the domain.

In terms of introductory knowledge the magneto caloric cycle will be explained including the adiabatic temperature rise. Figure 1.2.1 provides an overview of the different stages. The stages are ordered in time: Starting at A, continuing to D. Where the path from D to A may not be forgotten.

When the applied field is zero the magnetic moments are disordered, point A in figure 1.2.1. If the applied magnetic field becomes non zero the magnetic moments tend to align, which creates a more ordered state. In isentropic (adiabatic) conditions the magnetic entropy will lower as a consequence of the magnetic ordering. However, the total entropy must remain the same (or increase) according to the second law of thermodynamics. For the scope of this thesis the total entropy consists out of three main elements: magnetic, lattice and free electron entropy. Because the sum must remain the same, one of the entropies has to increase. In this case the lattice entropy will

increase. This causes the atoms in the material to vibrate more intensively, with an rise in temperature as effect, point B in figure 1.2.1. The free electron entropy is not altered by the changing applied magnetic field.

Now the temperature has increased above for example the ambient temperature, the current state can be maintained for a longer period of time. During this time period the material can cool down (not adiabatic), whilst enduring a magnetic field. This process is illustrated when moving from state B to C.

The following step in the cycle is removing the magnetic field. This in turn will increase the magnetic entropy. However, the same entropy law applies: the lattice entropy will increase and therefore the temperature of the material will drop. However, due to the heat removal the final temperature will be lower than the ambient temperature. (moving from point C to D in figure 1.2.1).

Maintaining the state of no applied magnetic field will allow the material to obtain the ambient temperature after which it reached its initial state again.

In the case of an truly adiabatic and steady state situation the temperature at the end of the cycle is the same at the beginning of the cycle. The ambient temperature or heat transfer from or to the ambient is not taken into account.

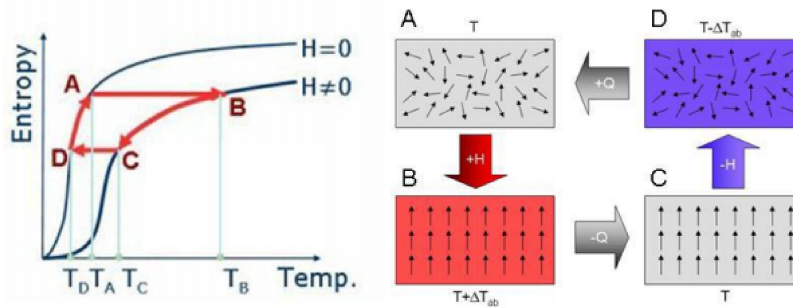


Figure 1.2.1: The magnetocaloric effect is shown here in a temperature entropy diagram and provided with illustrative figures to provide insight into the increase of the magnetic dipole moment.

1.3 ACTIVE MAGNETIC REGENERATOR

For an efficient use of the magneto caloric effect, usable temperature differences are required. Referring to the refrigerator example: an temperature difference between both sides of the refrigerator of approximately 15 Kelvin is required. Whereas the magneto caloric effect on itself can create an temperature step of approximately 5 Kelvin, depended on the magnetic field strength.

The magnetocaloric effect used in heat pumps is usually depended on permanent magnets as the magnetic field source. In order to create an high temperature span very cost intensive magnets would have to be used. These powerful magnets would create a high temperature change over one cycle. Next to this the high magnetic fields could provide mechanical challenges, which make the heat pump cost intensive again. Usually magnets, that are affordable, provide a magnetic field of 0.8 to 1.5T. These magnetic fields lead to a adiabatic temperature change in gadolinium of about 5K [7]. This temperature change is too low for the usual required temperature span which is in the order of 20 to 35 Kelvin. The most common way to obtain an higher temperature span created by a heat pump is to use a cycle that includes regeneration. The MCE must be used as an active component as suggested by Barclay in 1983 [8].

The main indicator of an active magnetic regenerator(AMR) is that all parts of the AMR simultaneously accept or reject heat to the heat transfer fluid. The fluid transport on its turns ensures the transfer of heat to internal neighbouring parts of the AMR or the heat exchangers. In order to obtain the regenerative effect a oscillatory fluid flow is applied. In this thesis a Brayton-like thermodynamic cycle will be used. A further detailed explanation will be given in chapter 5.

For this thesis the heat pumps will be configured in a cooling way: a finite volume will be cooled and heat will be rejected into a heat sink. One of the most relevant parameters is the cooling capacity. The cooling capacity is foremost dependent on the magneto caloric material that is used. Studies have shown limiting cooling capacities

when using gadolinium for practical applications [9] [10] and [11]. Next to this gadolinium is an expensive material. Different materials have been investigated for their MCE. In this thesis the use of $\text{Mn}_{1.25}\text{Fe}_{0.7}\text{P}_{1-y}\text{Si}_y$ as a substitute for gadolinium is investigated in a AMR setting. This material has remarkable magneto caloric promising with limit negative properties; it is relatively cheap and has a low environmental impact [12].

FUNDAMENTALS OF THE MAGNETOCALORIC EFFECT

The current chapter presents the thermodynamics of the magnetocaloric effect (MCE). This chapter prepares for the energy balance check, as will be presented in chapter 4. In order to obtain a proper energy balance a thorough understanding of the thermodynamics is required.

2.1 INTRODUCTION

The MCE is produced by a interaction between the spin system of the material and the change of internal magnetic field strength, H . The MCE is discovered for more than a century ago. All magnetic materials can produce a MCE, however, the magnitude of its effect varies strongly per material. The thermodynamics are related to the magnetocaloric material as the observed system. Therefore the magnetic field inside the magnetocaloric material is considered. The external magnetic field, related to the magnetic field source, is not considered. For this experiment volume and pressure are assumed constant.

When increasing the magnetic field strength in a soft-ferromagnet the electronic spins tend to align. The result is a, inevitably, lowering of the magnetic entropy. Depending on the boundary conditions; adiabatic or isothermal, the total entropy will decrease or remain constant. The total entropy can be written as the sum of several entropies: the magnetic, electronic and lattice entropy. The following expression as made by Pecharsky et al. 2001 [13], can be found:

$$S = S_{\text{mag}} + S_{\text{lat}} + S_{\text{elc}} \quad (2.1.1)$$

Due to its reversibility it seems obvious that this effect can be used as basis for a heat pump. In the 1920 and '30s the MCE was used in order to cool to temperatures close to the absolute zero (0.25K). This was done using a magnetic salt [14]. This thesis is primarily concerned with a magnetic heat pump at room temperature. The first experimental device using the MCE was a refrigerator presented by Brown 1976 [15].

2.2 ENERGY

The first law of thermodynamics for a closed system states that the internal energy of the magnetocaloric material will increase if heat is added or if work is performed upon the material. This law is usually written as follows:

$$du = \delta q - \delta w \quad (2.2.1)$$

In order to produce the MCE the magnetocaloric material has to be moved into the magnetic field. This results in a change of the magnetic field inside the material. Due to the magnetic field the material also gets magnetized; it will start to produce its own magnetic field. The work required to magnetize the magnetocaloric material can be written as:

$$dw = \mu_0 H dM \quad (2.2.2)$$

The system can be considered isentropic and adiabatic resulting in the following use of the second law of thermodynamics:

$$dq = T ds \quad (2.2.3)$$

Rewriting 2.2.1 into:

$$du = T ds + \mu_0 H dM \quad (2.2.4)$$

The derivative of the specific total entropy is defined in equation 2.2.11. The terms in this equation can be rewritten in terms of heat capacity as shown in equation 2.2.5 and 2.2.6.

$$c_H = \left(\frac{\delta q}{\delta T} \right)_H = T \left(\frac{\delta s}{\delta T} \right)_H \quad (2.2.5)$$

$$c_T = \left(\frac{\delta q}{\delta H} \right)_T = T \left(\frac{\delta s}{\delta H} \right)_T \quad (2.2.6)$$

Which finally will provide a more usable term for dq:

$$dq = c_h(T, H) dT + c_T(T, H) dH \quad (2.2.7)$$

Using the following Maxwell relation the latter equation, 2.2.6, can be rewritten as:

$$c_T = T \left(\frac{\delta s}{\delta H} \right)_T = \mu_0 T \left(\frac{\delta M}{\delta T} \right)_H \quad (2.2.8)$$

Now equation 2.2.7 can be rewritten as:

$$dq = c_h(T, H) dT + \mu_0 T \left(\frac{\delta M}{\delta T} \right)_H dH \quad (2.2.9)$$

Looking at equation 2.2.4 and 2.2.9 the internal energy can be rewritten as:

$$du = c_h(T, H) dT + \mu_0 T \left(\frac{\delta M}{\delta T} \right)_H dH + \mu_0 H dM \quad (2.2.10)$$

Equation 2.2.10 will later be used as a check for the energy balance. Next to this this expression can be rewritten in to a source term for heat, see paragraph 2.2.2.

2.2.1 ISOTHERMAL ENTROPY CHANGE

When considering the total entropy to be a function of the magnetic field strength and temperature the following total derivative of the entropy can be found

$$dS(T, H) = \left(\frac{\delta S}{\delta T} \right)_H dT + \left(\frac{\delta S}{\delta H} \right)_T dH. \quad (2.2.11)$$

The entropy change can be rewritten into: *De juiste vergelijkingen moeten nog genoemd worden

$$ds(T, H) = \left(\frac{\delta S}{\delta H} \right)_T dH = \mu_0 \left(\frac{\delta M}{\delta T} \right)_H dH \quad (2.2.12)$$

When the applied field varies, the internal field will also change. When considering isothermal conditions the isothermal entropy change can be defined as follows:

$$\Delta s = s_2 - s_1 = \int_{H_1}^{H_2} \left(\frac{\delta s}{\delta H} \right)_T dH \quad (2.2.13)$$

Using the maxwell relation, 2.2.8, equation 2.2.13 can be rewritten:

$$\Delta s = \int_{H_1}^{H_2} \mu_0 \left(\frac{\delta M}{\delta T} \right)_H dH \quad (2.2.14)$$

$$\Delta s = \int_{H_1}^{H_2} \frac{c_T}{T} dH \quad (2.2.15)$$

2.2.2 ADIABATIC TEMPERATURE CHANGE

In order to characterize the magnetocaloric material the adiabatic temperature change will be used throughout the thesis. This means that the temperature change is caused by the change of the magnetic field in the absence of heat flow. In this type of process, the adiabatic-isentropic process, the total specific entropy does not alter. This means that equation 2.2.11 is equal to zero. Using equation 2.2.6 the following relation can be found:

$$\left(\frac{\delta s}{\delta T}\right)_H = \left(\frac{\delta s}{\delta H}\right)_T = \mu_0 \left(\frac{\delta M}{\delta T}\right)_H dH \quad (2.2.16)$$

Which can be rewritten into the expression for adiabatic temperature change, using equation 2.2.3:

$$\Delta T_{ad} = -T \frac{\mu_0}{c_H} \int_{H_1}^{H_2} \left(\frac{\delta M}{\delta T}\right)_H dH \quad (2.2.17)$$

The two types of change can be represented in a T-S diagram as shown in figure 2.2.1.

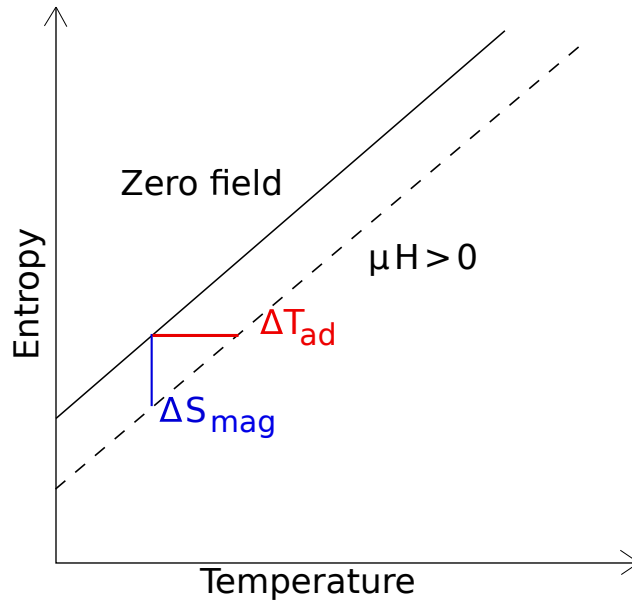


Figure 2.2.1: The magnetocaloric effect is shown here in a T-S diagram. The full line is the representative of the entropy of the material in a zero field situation and the dashed line in a non-zero field. The adiabatic temperature change is defined as the difference between two temperature points, with the same entropy. The difference in entropy at the same temperature is defined as the isothermal entropy change.

SOURCE TERM Rewriting equation 2.2.17 to obtain the source term of heat produced by the MCE:

$$\rho c_H \frac{dT}{dt} = -T \rho c_H \left(\frac{\delta M}{\delta T}\right)_H \frac{dH}{dt} \quad (2.2.18)$$

$$\dot{Q}_{MCE} = -T \rho c_H \left(\frac{\delta M}{\delta T}\right)_H \frac{dH}{dt} \quad (2.2.19)$$

2.3 CYCLIC OPERATION

The thermodynamic cycle in this case consists out of several discussed states, eventually ending up in the initial state. In order to describe such a process state functions can be used. The derivation of equation 2.2.10 is representing such a state function. In case of a cyclic operation the cyclic integral of the state function is zero. The internal energy represents the state function, then the first law of thermodynamics can be rewritten in the following form:

$$\oint dw = \oint dq = \oint T ds \quad (2.3.1)$$

As discussed in equation 2.2.2, the closed system can be rewritten into:

$$\oint dw = -\mu_0 \oint H dM \quad (2.3.2)$$

The product of the magnetization and the magnetic field can be rewritten as the cyclic integral of the state function.

$$\oint d(M \cdot H) = \oint M dH + \oint H dM = 0 \quad (2.3.3)$$

$$\oint M dH = -\oint H dM \quad (2.3.4)$$

This can than be further used to rewrite the last term of the internal energy:

$$\oint dw = -\mu_0 \oint H dM = \mu_0 \oint M dH \quad (2.3.5)$$

The internal energy, as described in equation 2.2.10, can now be calculated as follows using the derivation of the magnetic work as presented in equation 2.3.5.

$$\Delta u(t) = \int_{T_i}^{T(t)} c_H(T, H) dT + \int_0^{H(t)} T \mu_0 \left(\frac{\delta M}{\delta T} \right)_H dH - \int_0^{H(t)} \mu_0 M dH \quad (2.3.6)$$

This last equation is easy to implement hence the reason of discussing the cyclic operation. In table 2.3.1 the various terms of the internal energy balance are summarized.

Table 2.3.1: Description of the various energy terms.

Term	Description
$c_h(T, H) dT$	Representative of the internal heat
$\mu_0 T \left(\frac{\delta M}{\delta T} \right)_H$	The heat source term due to the changing magnetic field
$\mu_0 H dM$	The magnetic work term

MATERIAL PROPERTIES

The following chapter describes how the magnetic properties of gadolinium and $Mn_{1.25}Fe_{0.7}P_{1-y}Si_y$ are obtained. These properties will be used in the following chapter to create a 0D model for gadolinium. This model will use the thermodynamic relations as derived in chapter 2. At the end of this chapter the obtained material properties will be compared to the experimental determined properties for gadolinium.

3.1 TRANSITION TEMPERATURE T_C

In the previous chapter the MCE is explained. However the magnitude of this effect is mainly depended on material properties. For this thesis two materials are used that exhibit an significant MCE around room temperature namely gadolinium and $Mn_{1.25}Fe_{0.7}P_{1-y}Si_y$. The effect is usually the largest around the temperature where the material undergoes the magnetic phase change between being ferromagnetic and para-magnetic. This transition temperature is denoted by the Curie temperature T_C . The temperature is defined at which the spontaneous magnetization becomes zero [16].

T_C can be defined in various ways: determining the maximum isothermal entropy change or looking at the peak temperature of the specific heat. Both will be used to dimensionalize the numerical experiments. However these quantities may vary as a function of the magnetic field [13], [17].

3.1.1 1st AND 2nd ORDER TRANSITIONS

In general two types of phase transitions can be obtained, depending on the material properties: a first order and a second order phase transition. The typical phase transition of a ferro magnet is of second order. In the case where a structural transition together with the magnetic transition the phase may become first order. [18]. Other characteristic properties of first order transitions are: sharp and narrow peaks in magnetocaloric properties, very high or even infinite $\frac{\Delta S}{\Delta T}$ and $\frac{\Delta M}{\Delta T}$ and hysteresis. Following from the high derivatives the theoretical specific heat is infinite at the transition temperature. Due to the hysteresis of first order materials are prone to be neglected in MCE-studies. However a large δS and adiabatic temperature change are desired for high performance magnetocaloric heat pumps.

For second order transition the derivatives $\frac{\Delta S}{\Delta T}$, $\frac{\Delta M}{\Delta T}$ are discontinuous. The peak of the magnetocaloric properties is more wide and smooth and there is no latent heat around the transition temperature.

3.2 MATERIAL PROPERTIES OF GADOLINIUM

To determine the magnetic properties of a material the Mean Field Theory (MFT) can be used as described by Morrish [19]. The MFT is a combination of three models in order to determine the heat capacity, see equation 3.2.1. The Weiss-theory is used to obtain the theoretical magnetization and the magnetic contribution to the specific heat capacity. As a consequence the derivative of the specific magnetization with respect to temperature can be determined as well. The Debye-model is used to obtain the lattice contribution to the specific heat [20]. The third

model is the Sommerfeld model to account for the free electron contribution to the specific heat capacity [20]. Please note that this model provides the theoretical properties.

$$c = c_m + c_l + c_e \quad (3.2.1)$$

In this case the properties of gadolinium will be determined. In order to initiate these calculations several constants are to be collected, as presented in table 3.2.1

Table 3.2.1: The parameters for the mean field model for gadolinium [21] [22].

Parameter	Value	Unit	Description
T	280 ~ 330	K	Temperature range
H	0 ~ 1	T	Applied magnetic field strength range (Tesla)
N	$3.83 \cdot 10^{24}$	kg^{-1}	Number of atoms per unit mass
N_s	$3.83 \cdot 10^{24}$	kg^{-1}	Number of magnetic spins per unit mass
Θ_D	169	K	Debye temperature
T_c	293	K	Currie temperature
γ_e	$6.93 \cdot 10^{-2}$	$\text{J kg}^{-1} \text{K}^{-2}$	Sommerfeld constant
g_j	2	-	Lande factor
J	3.5	J(h)	Total angular momentum
ρ	7900	kg m^{-3}	Density
k_B	$1.38 \cdot 10^{-23}$	J K^{-1}	Boltzman constant
μ_0	$1.25 \cdot 10^{-6}$	$\text{m kg s}^{-2} \text{A}^{-2}$	Permeability of free space
μ_B	$9.274 \cdot 10^{-24}$	J T^{-1}	Bohr magneton

3.3 THE WEISS MEAN FIELD MODEL

As discussed the theoretical specific magnetization and its contribution to the heat capacity can be obtained using the Weiss model. The specific magnetization can be written as:

$$m = N_s g J \mu_B B_J(\chi) \quad (3.3.1)$$

The μ_B is the Bohr magneton. The latter parameter represents the Brillouin function. Which is defined as:

$$B_J(\chi) = \frac{2J+1}{2J} \coth\left(\frac{2J+1}{2J} \chi\right) - \frac{1}{2J} \coth\left(\frac{1}{2J} \chi\right) \quad (3.3.2)$$

$$\chi = \frac{gJ\mu_B\mu_0 H}{k_B T} + \frac{3T_c J}{T(J+1)} B_J(\chi) \quad (3.3.3)$$

As can be seen to solve these equations they have to be iterated to create a self-consistent solution. The to be calculated values are created in this set-up for a set of temperatures and applied magnetic field strengths. They are presented in table 3.2.1.

The magnetic contribution to the specific heat capacity is:

$$c_m = \mu_0 H \frac{\delta M}{\delta T} - \frac{1}{2} N_{\text{int}} \frac{(\delta M)^2}{\delta T} \quad (3.3.4)$$

In this case the mean field constant, N_{int} , is described as:

$$N_{\text{int}} = \frac{3k_B T_C}{N_s g^2 \mu_B^2 J(J+1)} \quad (3.3.5)$$

3.4 THE DEBYE & SOMMERFELD MODEL

The Debye model is used to determine the lattice contribution to the specific heat:

$$c_l = 9Nk_B \left(\frac{T}{\Theta_D} \right)^3 \int_0^{\frac{\Theta_D}{T}} \frac{x^4 e^x}{(e^x - 1)^2} dx \quad (3.4.1)$$

The Sommerfeld model is used to determine the last contribution: the free electron contribution:

$$c_e = \gamma_e T \quad (3.4.2)$$

3.5 THEORETICAL MATERIAL PROPERTIES

The above model can be implemented into Matlab®. The MCE will be shown at first in a 0D condition which will be discussed later in chapter 4. In this configuration the simulation will use theoretical material properties of Gadolinium. The justification will be done by comparing these properties with the experimental properties. Because of the main goal of the thesis the material properties are defined around T_C and room temperature.

3.5.1 HEAT CAPACITY

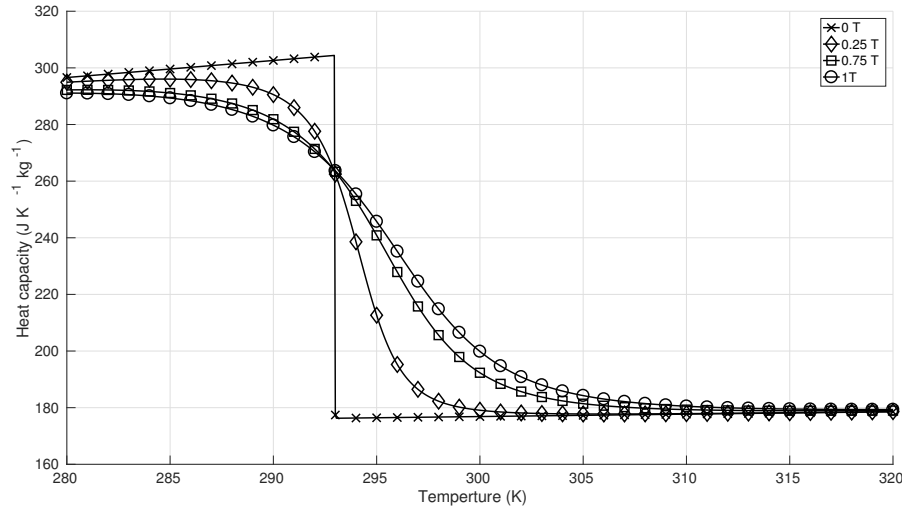


Figure 3.5.1: The heat capacity shown at various applied magnetic field strengths around T_C . The material of investigation: Gadolinium.

Around T_C the magnetic contribution to the heat capacity becomes significant. In this temperature region the effect of the applied magnetic field is very clear, see figure 3.5.1. The specific heat varies when the applied field is varied. Because of the high efficiency of the MCE around T_C , this effect is important to take into account when comparing numerical results to experimental results. At a zero field there is a strong discontinuity. This is due to the singularity of the hyperbolic cosine in these conditions. Moving away from 0 Tesla, the functions become smoother.

3.5.2 MAGNETIZATION

The magnetization is a vector quantity which is defined as the magnetic dipole moment. The specific magnetization is plotted against the temperature, see figure 3.5.2. Also in this case various field strengths are used. Just as in case of the heat capacity, the effect of the applied magnetic field is clearly visible around T_C . The effect of the

applied magnetic field in the temperature region below 280 Kelvin is negligible. However at the Curie temperature and higher the magnetic dipole moments ordering will decrease. The alignment of the dipoles is very messy. Increasing the applied magnetic field will align the dipoles more.

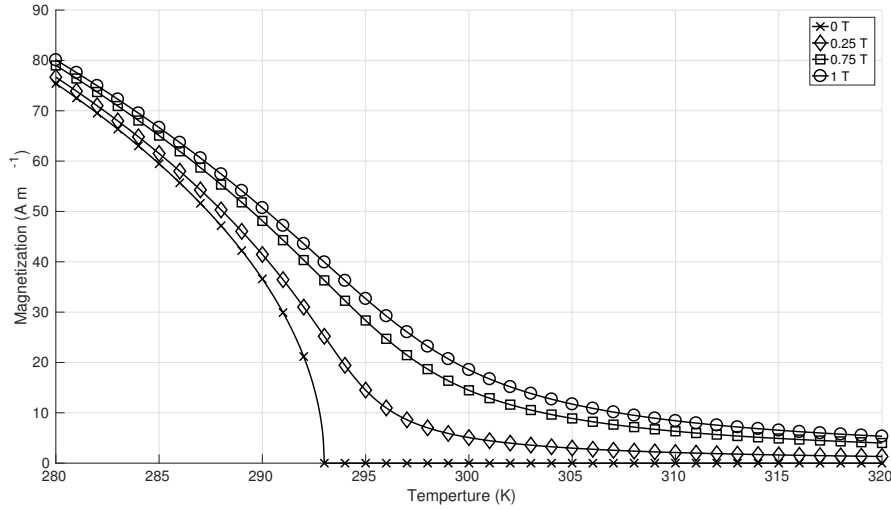


Figure 3.5.2: The internal magnetization shown at various applied magnetic field strengths around T_C . The material of investigation: Gadolinium.

The effect of the hyperbolic cosine from the model is again very visible at 0T. The hyperbolic cosine behaves asymptotic at 0T and temperatures above T_C .

The Curie temperature indicates the transition temperature: the phase transition from ferromagnetism to paramagnetism. In case of the absence of the magnetic field the magnetization of the paramagnetic material is zero. Due to higher applied magnetic fields the transition temperature is shifted, to higher temperatures. The lines appear to converge towards zero far beyond 330 Kelvin. This means that an increase in temperature will not greatly affect the magnetization, when for example the magnetic field is varied for a MCE.

3.5.3 TEMPERATURE DERIVATIVE OF MAGNETIZATION WITH RESPECT TO TEMPERATURE

In the heat source equation 3.5.1, the derivative of the magnetization with respect to temperature, $\left(\frac{\delta M}{\delta T}\right)_H$ plays an important role. For this reason this term is interesting to discuss and visualize around T_C .

$$\dot{Q}_{MCE} = -T\rho\mu_0\left(\frac{\delta M}{\delta T}\right)_H \frac{dH}{dt} \quad (3.5.1)$$

Due to the asymptotic behaviour of the magnetization the derivative is also discontinuous, see figure 3.5.3. The amplitude of the derivative at zero field is very high. According to Kitanovsky [6] this value is expected to be much lower. The asymptotic behaviour is not a problem since the value of the derivative drops drastically when the applied magnetic field is non-zero. In figure 3.5.2 the applied magnetic field begins to affect the magnetization around T_C . This can be seen again in the derivative. No matter how high the magnetization the derivative peaks at T_C . Due to this increase in value the MCE is most noticeable around T_C .

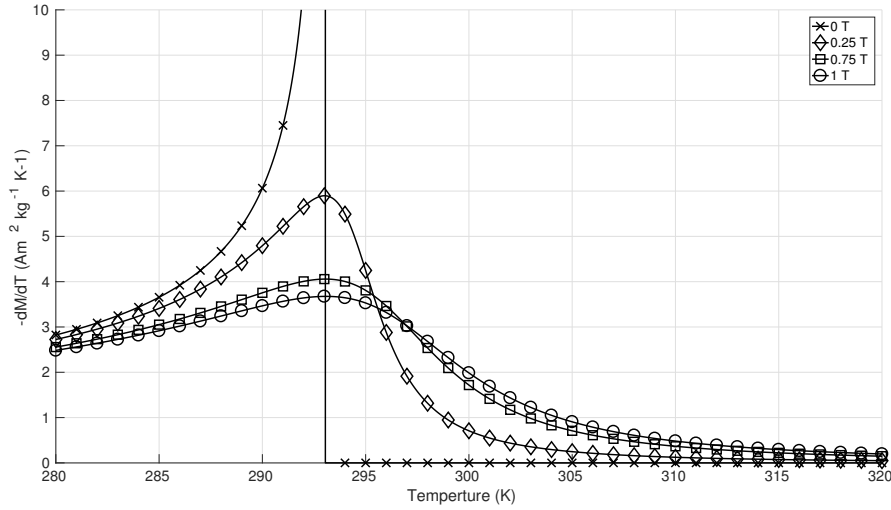


Figure 3.5.3: The derivative of magnetization with respect to temperature shown at various applied magnetic field strengths around T_C . The material of investigation: Gadolinium.

3.6 MATERIAL PROPERTIES OF $Mn_{1.25}Fe_{0.7}P_{1-y}Si_y$

The use of gadolinium as a MCE-material has the main disadvantage of being expensive. Next to this gadolinium is only effective in a specific temperature range which can be disadvantageous if a large temperature span is required. The effectiveness of a heat pump which relies upon the MCE with one MCM is depended on the desired temperature span. During the operation of an AMR a temperature profile is established throughout the device. Due to this temperature profile parts of the AMR are at a temperature that are, temperature wise, far away from the materials Curie temperature. The magnetocaloric effect in these parts will be much lower and decrease the performance in terms of entropy or temperature change of the AMR. In order to overcome this problem several materials with specific temperature ranges can be used in series. Several experimental and numerical studies have proven this concept [23], [24],[25].

As mentioned earlier materials that exhibit a first order behaviour in a magnetic field display latent heat. Nowadays the preferred approach is to use this latent heat to reach large ΔS and ΔT_{ad} values. Various material families are known and studied that display a so-called 'giant MCE'. The materials being: $Gd_5(Si,Ge)_4$, $La(Fe,Si)_{13}$ and the $MnFe(P,X)$ family with $X = As, Ge$ or Si [12]. In this thesis the use of $Mn_{1.25}Fe_{0.7}P_{1-y}Si_y$ is being investigated as a material for an AMR set up. The use of 'y' indicates that several compounds can be created. In this case $y = [0.49, 0.50, 0.51, 0.52]$. This compound shows remarkable magnetic and MCE properties whereas by varying the y value the transition temperature can be altered [12]. Various material properties are obtained via direct measurements as done by [12] and can be used to determine and estimate the values for other magnetic field strengths than determined by Yibole(2014) et. al. The determined properties are later used in numerical experiments, see chapter 6.

3.6.1 HEAT CAPACITY

Due to the lack of consistent heat capacity data, results of direct measurements of the magnetocaloric effect in $Mn_{1.25}Fe_{0.7}P_{1-y}Si_y$ are used to obtain the heat capacity. No hysteresis is assumed for this model which can be justified by the found limited hysteresis effect as found by Bruck [12]. This assumption leads to the justification of the irreversibility of the MCE.

The direct measurements provide entropy change data see figure 3.6.1a and 3.6.1b. This data can be used to

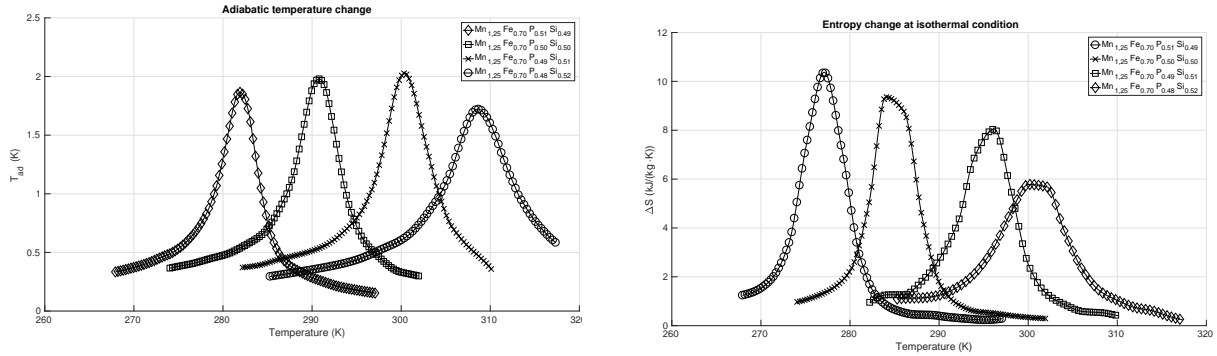
determine the heat capacity, according to simple thermodynamics:

$$\Delta S = \int_1^2 \left(\frac{\delta q}{T_0} \right)_{intrev} = \frac{1}{T_0} \int_1^2 (\delta q)_{intrev} \quad (3.6.1)$$

$$\Delta S = \frac{q}{T_0} [\text{J}/(\text{kg K})] \quad (3.6.2)$$

In this case T_0 stands for the temperature at which the entropy change has been measured. The data used is created at a magnetic field of 1 Tesla. Now the total heat per kilogram can be derived from equation 3.6.2.

Next to the entropy change the adiabatic temperature change has been measured and reported. This in turn can be used to once again determine the total heat per kilogram.



(a) The adiabatic temperature change at a field variation to 1 Tesla.

(b) The isothermal entropy change at a field variation of 1 Tesla.

$$q = c_p \cdot \Delta T_{adiabatic} [\text{J}/(\text{kg K})] \quad (3.6.3)$$

Rewriting equation 3.6.2 and 3.6.3 provides an expression for the heat capacity:

$$c_p = \frac{\Delta S \cdot T_0}{\Delta T_{ad}} \quad (3.6.4)$$

Resulting in the following figure for the heat capacity at 1 Tesla.

The first thing to notice is the immense change of heat capacity when the compounds are being held in a magnetic field. Further to notice are the starting values, suggesting a higher heat capacity before T_C and the aft T_C values, suggesting a lower heat capacity after the Currie temperature. This is also seen in gadolinium.

The maximum values in heat capacity are different from the values for the adiabatic temperature change. If a temperature profile is applied upon $\text{Mn}_{1.25}\text{Fe}_{0.7}\text{P}_{1-y}\text{Si}_y$ it could be beneficial to ensure that both temperatures are within the domain temperature wise.

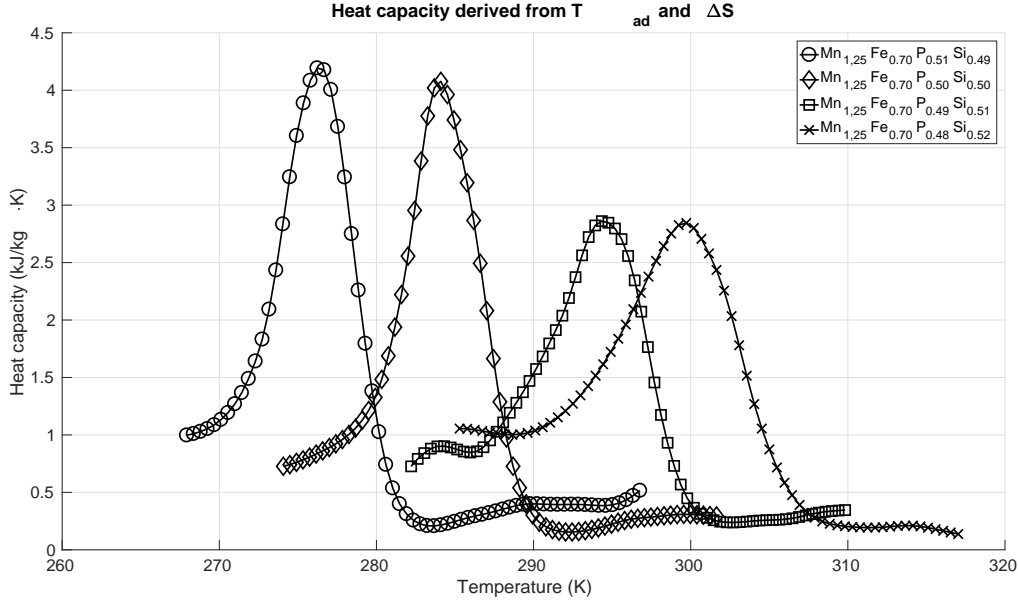


Figure 3.6.2: The heat capacity derived from the adiabatic temperature change and isothermal entropy change at 1 Tesla.

HEAT CAPACITY DETERMINATION USING $\frac{dM}{dT}$ According to the thermodynamics of the magneto caloric effect the heat capacity can also be determined by using the magnetization data. The heat capacity change can be determined using the rewritten form of equation 2.2.17. This equation provides the adiabatic temperature change due to the magnetocaloric effect. However, the latent heat is not included in this calculation. Using the magnetization data an estimate can be made of the influence of the latent heat upon the adiabatic temperature change. Which in turn provides a more accurate estimate of the heat capacity.

$$c_p = \frac{m\mu_0}{T_{ad}} \cdot T \cdot \left(\frac{\delta M}{\delta T} \right)_H \cdot H \quad (3.6.5)$$

Equation 3.6.5 requires the derivative of the magnetization with respect to temperature. Using the experimental data this derivative can be determined which in turn provides with again the heat capacity, see figure 3.6.3.

The heat capacity is now peaking at 3000~ 2500 J/kg K instead of 4200. The first method of determining the heat capacity is based upon the entropy change and temperature change. However the second method is depended on the magnetization curve. The second method does not incorporate the latent heat present during the magnetization, which in turn provides a lower heat capacity.

The height of the heat capacity can be justified by considering the large entropy change whilst maintaining a relative low temperature change. Even when isolating the entropy change from the heat capacity calculation provides a high heat capacity.

In essence are both method exactly the same considering the thermodynamics. The reason to calculate the heat capacity is to estimate the magnitude of the latent heat. This latent heat is also measured during the adiabatic temperature changes and is one of the reasons this material is so promising [12].

The above determined heat capacities are at 1 Tesla. For other magnetic field strengths the heat capacity is assumed as described in the following. This is done by slightly imitating the behaviour of gadolinium to incorporate the effect of the different magnetic states of the material before and after T_C . At zero Tesla at temperatures before T_C a value of 900J/Kg K is assumed as heat capacity, where after T_C a value of 450 J/Kg K is assumed. The same values are assumed for temperatures away from T_C at non zero magnetic field strengths.

Values for the heat capacity in between the two magnetic states are assumed to be on a linear slope in between the two given heat capacity functions. This is illustrated in figure 3.6.4 for clarity.

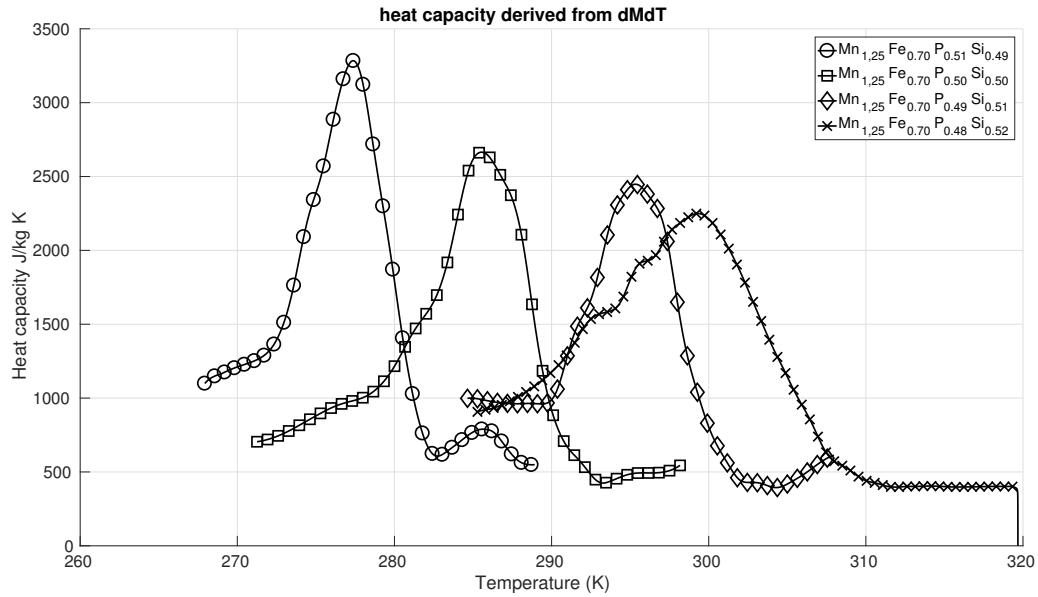


Figure 3.6.3: The heat capacity derived from the magnetization change and adiabatic temperature change at 1 Tesla.

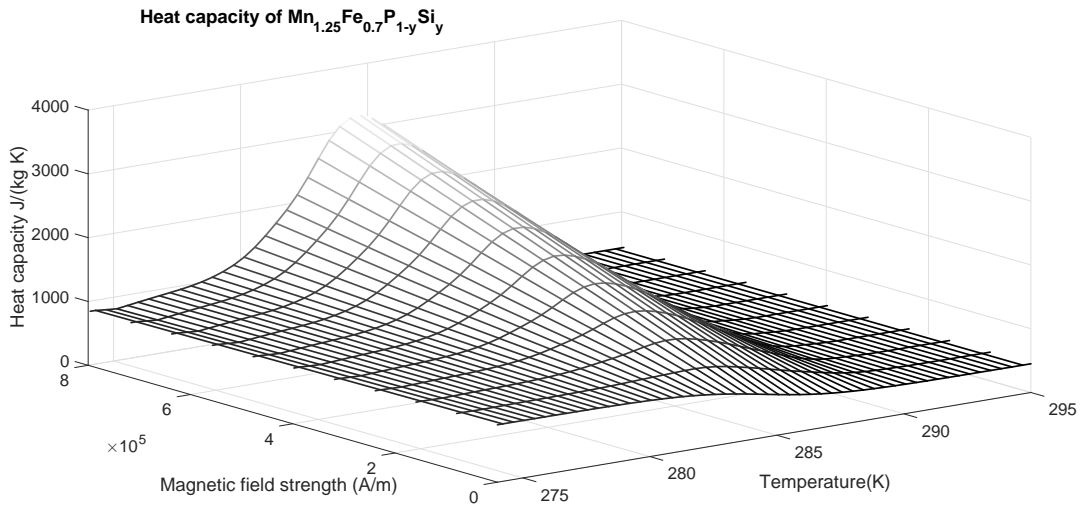


Figure 3.6.4: 3D heat capacity plot for $Mn_{1.25}Fe_{0.7}P_{1-y}Si_y$. The heat capacity is interpolated between the two known C_p curves ($H = 1T$ and $0T$).

3.6.2 MAGNETIZATION

The magnetization of the material plays an important role for the magnitude of the magneto caloric effect. The magnetization has been introduced in the previous part for calculating the heat capacity. However, literature provides a magnetization curve for a magnetic field strength of 1 Tesla, therefore the magnetization has to be estimated for other external field strengths. The assumption is that the application of the external magnetic field happens rather quickly thus the influence of the magnetization curve at other field strengths on the MCE can be neglected. Next to this the internal magnetization (Am^2kg^{-1}) of the material is zero if the external magnetic field is also zero

Tesla. The internal magnetization values in between zero and 1 Tesla are assumed to be on a linear interpolation field as shown in figure 3.6.5.

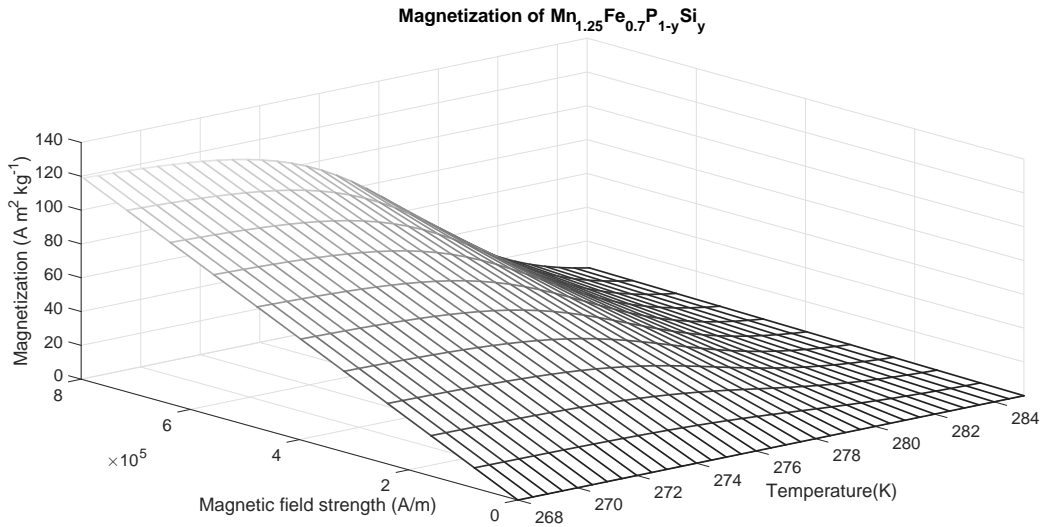


Figure 3.6.5: 3D magnetization plot for Mn_{1.25}Fe_{0.7}P_{1-y}Si_y. The magnetization is interpolated between the two known C_p curves ($H = 1\text{T}$ and 0T).

LATENT HEAT AND DERIVATIVES

In order to create a heat source function that behaves more or less predictable the internal magnetic field curve is imitated with a hyperbolic tangent. Retrieving data from the literature provides no smooth curve, and therefore the derivative is not smooth either. This in turn provides a heat source function that behaves not as expected when looking at the literature. To overcome this effect imitation functions are used.

When the adiabatic temperature is calculated using these imitation functions the magnitude of the MCE is too low. This is due to the fact that the thermodynamics describe second order behaviour more accurately since no latent heat is involved. To accommodate for the missing latent heat, the magnetization curves are slightly steepened. This in turn provides for higher derivatives and a more appropriate adiabatic temperature change. The result of this approach will be discussed in chapter 6.

3.6.3 DENSITY AND THERMAL CONDUCTIVITY

Other material variables required to solve for the heat transport equations are: thermal conductivity and density. By private communication with prof. van der Meer, these values are assumed constant and independent of magnetic field strength or temperature. The thermal conductivity is assumed to be $44.2476 \frac{\text{W}}{\text{m}\cdot\text{K}}$ and the density is assumed to be $5657.2 \frac{\text{kg}}{\text{m}^3}$. These values are derived from taking an average over the values taken from each individual part of the compound weighted by their fraction.

0D-MODEL

In the previous chapters two main subjects were introduced: the magnetocaloric effect and ways to find the material properties. This chapter will discuss the implementation of and evaluate these subjects. Previous studies at the University of Twente have found an inconsistent energy balance, this part is devoted to investigating this inconsistency. In the end the energy balance is discussed. Following chapters will concern the description of a 2D model and the use of other materials.

4.1 MODEL SET UP

In order to practice the magneto caloric effect in a numerical manner the most easy way to investigate the MCE is to create an 0D model. This will provide helpful insight in the energy contributions of each part of the internal energy balance and to validate whether the energy balance is consistent. The most simple setting to use is if adiabatic conditions are applied; no heat is added or lost from external sources other than the heat source term due to the MCE. This way only equation 4.1.1 is under investigation which represents the energy balance. This equation has been derived earlier in chapter two, see equation 2.2.10. Aspects such as the geometry, the position or orientation of the applied magnetic field, hysteresis and material inconsistencies are not taken into account.

$$du = c_h(T, H) dT + \mu_0 T \left(\frac{\delta M}{\delta T} \right)_H + \mu_0 H dM \quad (4.1.1)$$

4.1.1 NUMERICAL IMPLEMENTATION

The derived formulas for the material properties, see chapter 3, and the MCE, see chapter 2 are implemented into Matlab. Two distinctive parts can be identified: the solution script and the material property script. For this experiment gadolinium is used as the MCM.

The problem at hand is not analytically solvable and is time depended. The use of an explicit Runge-Kutta scheme is used, codename by Matlab: *ode45*. The system is evaluated as 'non-stiff' which justifies the use of this scheme. However this scheme has a medium accuracy as presented by the Matlab Documentation. The main goal of this experiment is to prove the consistency of the energy balance. The consistency of the energy balance could be depending on the time-stepping of the solver algorithm. A temporal study will therefore be used at which the error in the energy balance will be studied.

In order to still gain a quantitative solution, a variation in time-steps has to be made. This variation will show to what extend the solution is depended on the time stepping and therefore the accuracy of the numerical scheme. However when the time stepping becomes small the computational time will be estimated to be very long. Therefore a relative error in the energy balance will be set at the order of $1 \cdot 10^{-5}$.

Previous studies at the University of Twente have used a dataset for the material properties during the calculation process. As mentioned earlier the material properties are mainly depended on the applied magnetic field and temperature. In this study the solution scheme will be accompanied with a material property script.

The material property script will provide the values of the specific material properties such as magnetization and heat capacity. These values can be used by the solution scheme of the MCE. The solution scheme provides the conditions from which the script can calculate accurate material properties.

MATERIAL PROPERTY SCRIPT The heat capacity and the internal magnetization of gadolinium are depended on the applied magnetic field and current temperature. In order to obtain the corresponding values for these variables the script that determines these values requires the applied field and current temperature. The current temperature will be provided by the solution scheme. The mean field theory as described in chapter 3 is implemented into this script. By using both the solution and material script the solution will be calculated by using the proper material property values.

4.1.2 MODELLING THE MAGNETIC FIELD

In order to create an numerical magnetic field a unit step function was used, see equation 4.1.2. The step function has the ability to simulate an almost instantaneously change in magnetic field strength. This is done using two step functions in series: one for magnetization and the other for demagnetization. This magnetic field will be the field where the material will respond to; geometry or material defects will not be modelled.

$$H(t) = \frac{1}{2} + \frac{1}{2} \tanh(kt) \quad (4.1.2)$$

Due to the nature of implementing, the step function as presented the magnetic field is not zero at the beginning and end of the simulation, therefore extra time is added before the step functions kick in. Next to this extra time is added after the magnetization step to show the adiabatic behaviour of this system. During this extra time the magnetic field strength does not change and therefore the system will come to a temporary rest at its newly acquired temperature. Since the system is adiabatic no heat losses will be implemented or expected in the result.

Table 4.1.1: Numerical applied magnetic field timings.

Parameters	Value [s]
Total period	0.1
(de) Magnetization time	0.01
Mid time	0.06

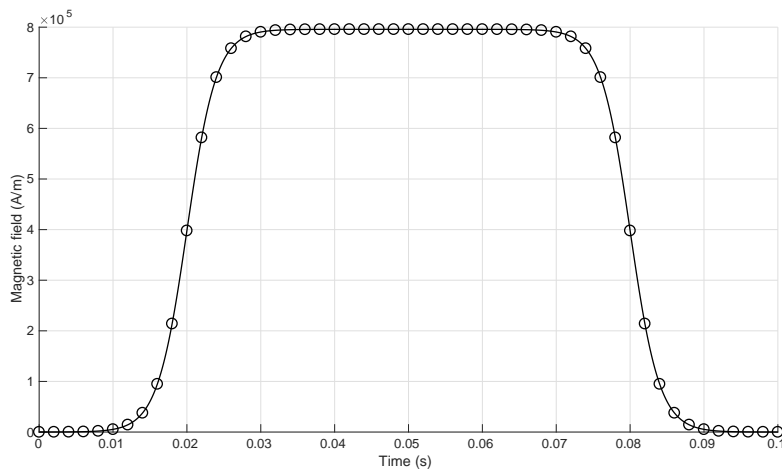


Figure 4.1.1: The applied magnetic field. The field strenght varies from 0 to 1 Tesla. The value in the graph is converted to SI units, using μ_0 .

The derivative of the applied magnetic field is present in the heat source and therefore required in the numerical scheme. This is implemented as 4.1.3.

$$\frac{dH}{dt} = k \frac{1}{2} \operatorname{sech}^2(kt). \quad (4.1.3)$$

The unit step functions describe only a part of the cycle. The same step is used only a delay later and multiplied by -1. This will provide a symmetrical function shape which in turn ensures cyclic behaviour in its most simple form: returning to the initial state.

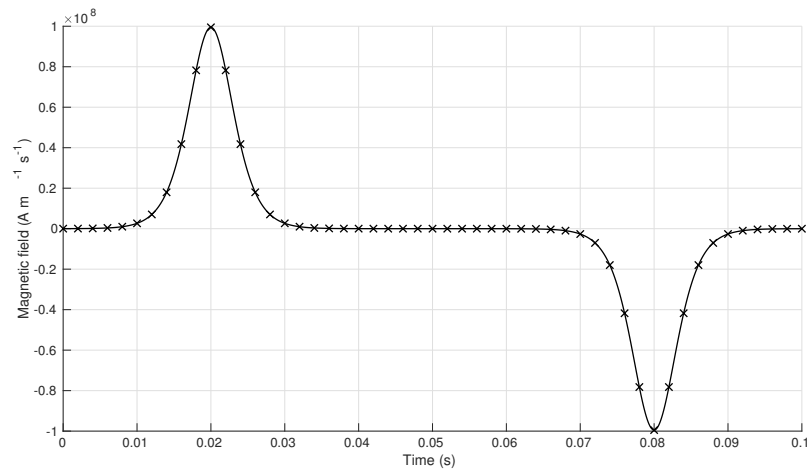


Figure 4.1.2: The derivative of the applied field plotted against the period time.

4.2 RESULTS AND DISCUSSION

The adiabatic temperature change realized in this model is as expected around 5.5K, see figure 4.2.1. The temperature remains at a constant value which implicates no heat loss. After de-magnetization the temperature reaches its original temperature. This indicates that the model accurately reacts upon the applied magnetic field and its other boundary conditions. This figure has been acquired at low time-stepping.

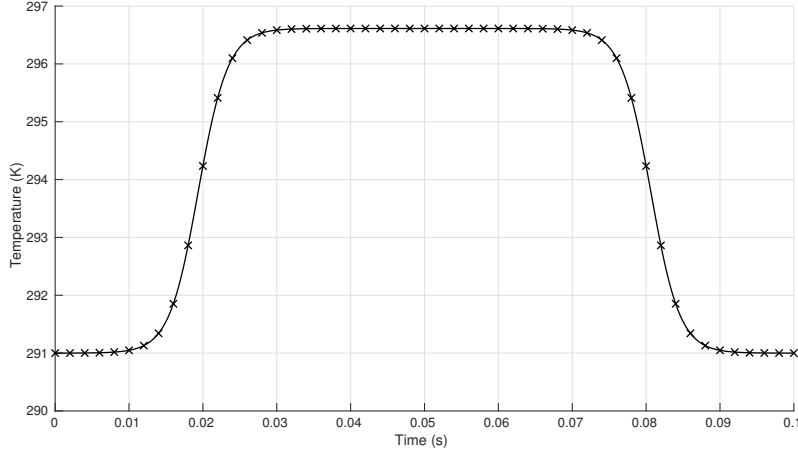


Figure 4.2.1: The adiabatic temperature change plotted against time. The model was set around T_C . This condition makes for a clear change in temperature on macro scale.

Every term of the the energy balance as presented in equation 2.3.6, repeated at equation 4.2.1, can be determined separately and are shown in figure 4.2.2. The heat source term experiences the highest energy difference. The temperature change is the largest contributor for the internal energy to raise. The magnetic work energy however is negative. In order to magnetize the material, energy is taken up by the material.

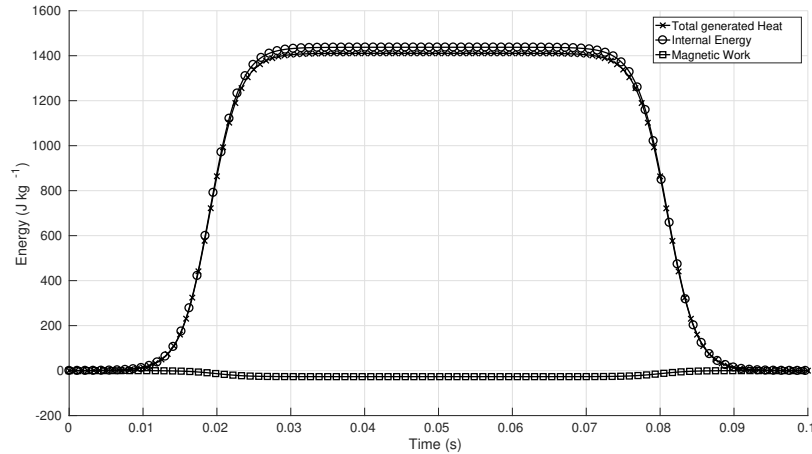


Figure 4.2.2: The energies plotted over time. Every line represents a term of the energy balance.

$$\Delta u(t) = \int_{T_i}^{T(t)} c_H(T, H) dT + \int_0^{H(t)} T \mu_0 \left(\frac{\delta M}{\delta T} \right)_H dH - \int_0^{H(t)} \mu_0 M dH \quad (4.2.1)$$

In order to prove that the thermodynamics are consist of the MCE the internal energy balance was evaluated at a small time-step. Every part of the energy balance can be calculated and plotted versus time. See figure, 4.2.2.

$$\text{error}[-] = \left(\frac{\int_{T_i}^{T(t)} c_H(T, H) dT}{\left(\int_0^{H(t)} t \mu_0 \left(\frac{\delta M}{\delta T} \right)_H dH \right) + \left(\int_0^{H(t)} \mu_0 M dH \right)} \right) \quad (4.2.2)$$

Equation 4.2.2 can be plotted, see figure 4.2.3. The relative error has not the same value throughout the entire period. This is due to numerical effects; at the the times the slope of the error is higher than 0, the (de)magnetization kicks in. The relative error is evaluated at half the total period, $t = 0.05\text{s}$. The $\frac{dH}{dt}$ is zero here and there is no change in state. The value of the error is $3.82 \cdot 10^{-5}$ at this time.

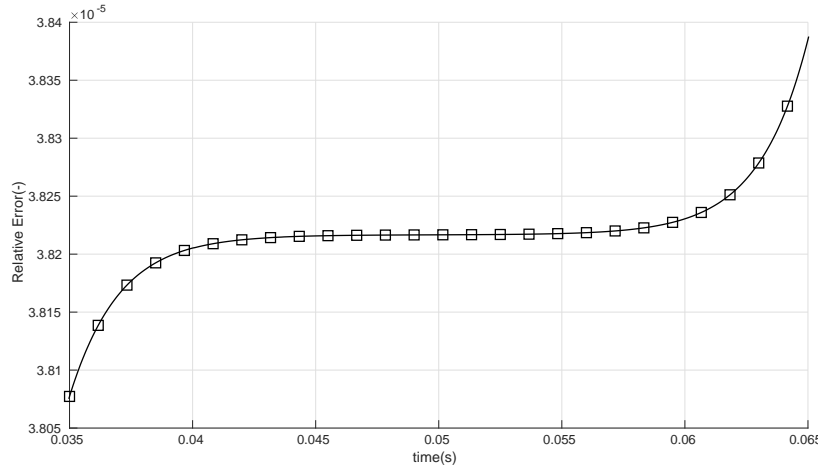


Figure 4.2.3: The error with respect to the internal energy plotted against time.

4.2.1 TEMPORAL STUDY

The magneto caloric effect is a time depended phenomena and can be calculated using various time-steps in the numerical solution scheme. The accuracy of the solution and therefore the energy balance seems to be depended on the time-stepping. Various time-steps have been used to calculate the energy-balance-error and are shown in table 4.2.1. The error seems to decrease towards engineering and scientific standards as the time step also decreases. This justifies the statement of the time-dependency of the MCE and the accuracy being depended on the time step.

Table 4.2.1: The error as calculated in equation 4.2.2, displayed against the time-stepping.

Time Step (s)	Error(-)
0.01	0.99
0.005	0.89
$1 \cdot 10^{-3}$	$4.40 \cdot 10^{-3}$
$5 \cdot 10^{-4}$	$3.75 \cdot 10^{-4}$
$1 \cdot 10^{-4}$	$1.88 \cdot 10^{-4}$
$5 \cdot 10^{-5}$	$3.82 \cdot 10^{-5}$

4.2.2 DISCUSSION

As can be seen in the previous section the energy balance error is below the engineering standard of $1 \cdot 10^{-3}$ and somewhat above the scientific standard of error of $1 \cdot 10^{-6}$. In this study it was found that the error decreases with smaller time steps. Therefore it is assumed that the energy balance is consistent only that the solution is depended on the time step. This in turns justifies the assumption that the thermodynamics are consistent as well. The accuracy of the solution seems to be depended on the time step size used in the solver.

However previous work at the University of Twente shows an in consistency in the energy balance [26] and [27]. Looking at the magnitude of their error it seems that the magnetic work has not been taken into account. When not taking the magnetic work into account at the error calculation the magnitude of this error resembles the error found in previous work.

Looking at the material properties of gadolinium at a low magnetic field strength these properties tend to be discontinuous. The model contains a hyperbolic cosine which at 0T magnetic field strength and the Curie temperature resembles a step function. Previous studies have used material property (heat capacity and magnetization) tables produced at various magnetic field strengths. When performing a calculation values for the missing magnetic field strengths where interpolated. However, interpolating at low magnetic fields could lead to improper material properties comparison to the original modelled values. The interpolation mechanism probably did not account for the relatively discontinuous material properties. Using the interpolated values for the material properties could have influenced the dis-balance in the energy equation.

ACTIVE MAGNETIC REGENERATOR

The previous chapter discussed the mechanism of the MCE and proved its energy balance. The current chapter will discuss the graded AMR, the numerical set-up and several parameters in general. The numerical set-up will be validated using literature.

5.1 2D MODEL - GADOLINIUM

As discussed the AMR provides for a higher efficiency in terms of heat transport than a cascade system or otherwise [18], [28].

For an experimental set-up it is desirable to have proper dimensions which could lead to experimental results that have considerable meaning. Obtaining these dimensions could be done via a numerical study. The main goal of this study is to provide such dimensions. This part of the thesis consists out of two parts: the first part discusses and studies the effect of the temporal and spatial resolution in a numerical scheme and the second part one important variable: the utilization factor. This factor will be explained later. This factor plays an important role in designing a experimental set-up consisting out of the $Mn_{1.25}Fe_{0.7}P_{1-y}Si_y$ material family. The first part consists out of a model of an AMR modelled in Comsol. The material used in this model is gadolinium. The reason for this material is that various studies both numerically and experimentally have been conducted and using the outcome of those studies can provide insight in the performance of the numerical set-up. Performing a temporal and spatial study provides helpful insight in to the accuracy of the outcome with respect to the previous studies versus computational time.

The second part investigates the behaviour of $Mn_{1.25}Fe_{0.7}P_{1-y}Si_y$ in an AMR setting. For this study one variables are studied resulting in an recommendation for an experimental set-up. Most of the dimensions are determined by an study performed by Paolo et. al. [29].

The AMR contains a porous structure of a magnetocaloric material. Through this porous structure a heat-transfer fluid is pumped with an oscillatory velocity pattern depending on the magnetization state. The AMR has two functions in a magnetic refrigerator: it works as the heat regenerator as the refrigerant. In general 4 steps of the AMR operation can be identified. These steps are in general analogue to the vapour-compression refrigerator cycle. These steps are:

- *Magnetization* The domain is exposed to an external magnetic field. Therefore the magnetization derivative becomes positive and the magnetocaloric effect occurs. This leads to an temperature increase due to adiabatic conditions. See figure 5.1.1a.
- *Fluid flow* Now the MCM is heated up it can be cooled by letting a fluid flow from the cold side, or cold-heat exchanger, to the hot side removing the heat from the MCM. The removed heat is either transported to another part of the MCM or dumped at the hot-heat exchanger. See figure 5.1.1b.
- *De-magnetization* The applied external field will no be removed from the domain. As explained in the thermodynamics of the MCE the temperature in the AMR is lowered. See figure 5.1.1c.

- *Fluid flow* also called hot-blow: fluid is moved from the hot heat exchanger through the AMR. This fluid is cooled by the AMR and eventually dumped into the cold heat exchanger. This last step removes heat from the cold side. Now the cycle is complete. See figure 5.1.1d.

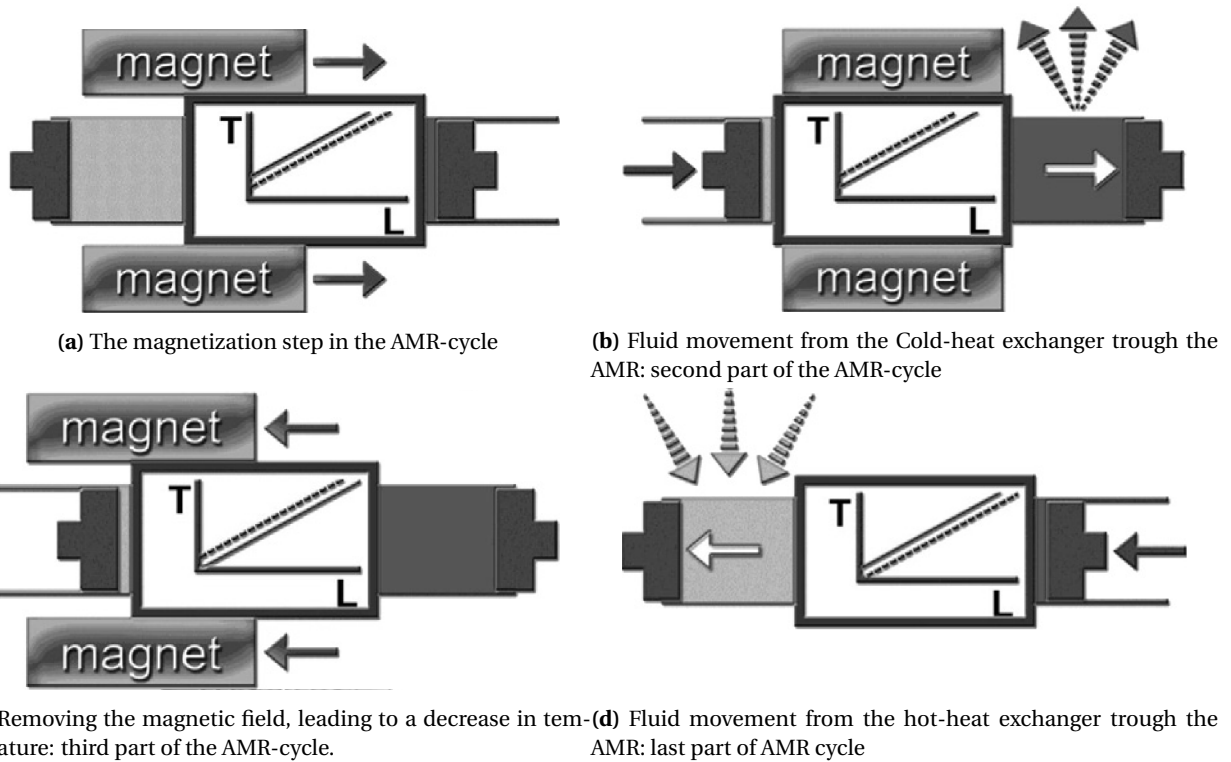


Figure 5.1.1: Figure used from [30]

The AMR-cycle can be described via an T-S diagram as showed in figure 5.1.2. This figure describes the AMR cycle at a given point in the regenerator. The entropy is considered as the total entropy of a given point including both the solid and the fluid.

The cycle starts with the magnetization as displayed in figure 5.1.1a. First the MCM is adiabatically exposed to a magnetization step. The fluid movements are displayed from B to C and D to A, which are displayed in figure 5.1.1b and 5.1.1d. Where the entropy is changing, however the temperature alters very little. The demagnetization step is removed in process C to D and is done adiabatically, which also is displayed in figure 5.1.1c.

Concluding, the physical problem of the AMR-cycle includes several aspects: a regenerator matrix made of gadolinium, a oscillatory flow of a heat transfer fluid and the interaction between a temporally changing magnetic field.

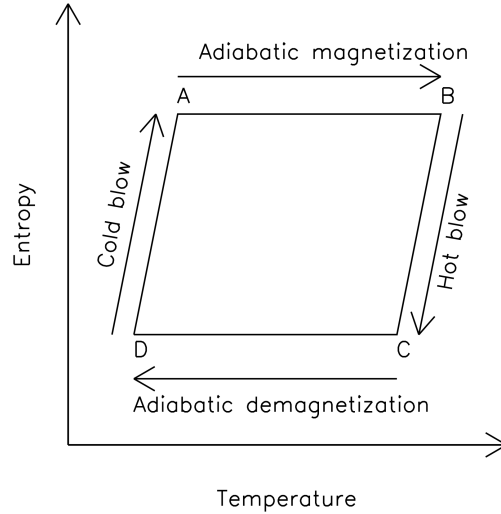


Figure 5.1.2: Every individual process of the AMR cycle. The schematic in this figure represents the T-S-diagram of each process for an infinitesimal part of the regenerator [18].

5.2 MODEL DESIGN

For the validation the theoretical cooling capacity and maximum temperature span of an AMR device using gadolinium are under investigation. Previous work of master students has delivered a 2-D model of an AMR device based on a regenerator with parallel plates of gadolinium modelled via the mean field theory [27].

The main goal of this part of the study is to investigate a proper spatial and temporal resolution. Various other work has been done on a parallel plate AMR containing gadolinium, [18], [8],[17], [9]. These provide parameter studies both in numerical and experimental set-ups.

The domain consists out of a simplified parallel plate AMR-set up, see figure 5.2.1. It is a two-dimensional model and simulates half a replicating cell. The cell consists out of half a plate of MCM and half a fluid channel. The x-direction is parallel to the plates, which also is indicative for the fluid flow. The y-direction is perpendicular to the plates. The z-direction is not represented by the model, hence its 2D-character: the cell is assumed to have an infinite width.

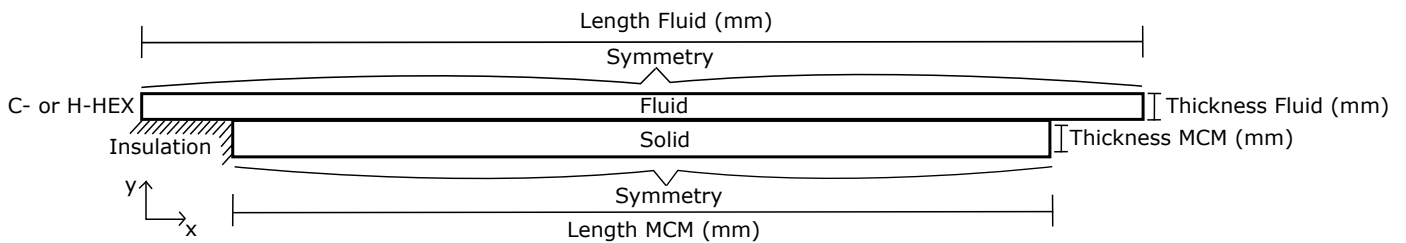


Figure 5.2.1: Numerical 2D domain, representing the AMR.

The approximation can be assumed sufficient for the flow but could be insufficient in terms of the thermal coupling to the ambient via boundary conditions. Heat losses are not assumed in this original model.

Various boundary conditions are displayed in figure 5.2.1. The cold-heat exchanger in a no load condition is modelled as a outflow boundary condition. When fluid moves in the positive x-direction the fluid has the temperature as calculated at that boundary condition. However, when fluid moves in the negative x-direction it could present a different temperature to this boundary condition. The boundary condition will then take the new temperature. This way a volume is represented that behaves adiabatically but is able to alter its temperature depending on the systems performance. This leaves the contact between the fluid and solid as a thermally coupled inner boundary. The governing equations of the thermal system are:

$$\frac{\delta T_f}{\delta t} = \frac{k_f}{\rho_f c_f} \left(\frac{\delta^2 T_f}{\delta x^2} + \frac{\delta^2 T_f}{\delta y^2} \right) - (u \cdot \nabla) T_f \quad (5.2.1)$$

$$\frac{\delta T_s}{\delta t} = \frac{k_s}{\rho_s c_s} \left(\frac{\delta^2 T_s}{\delta x^2} + \frac{\delta^2 T_s}{\delta y^2} \right) \quad (5.2.2)$$

The subscripts denote the solid and fluid by s and f. The fluid equation, 5.2.1, consists out of two terms: the diffusion term and convective term. The velocity field is denoted by, u, is obtained by solving the Navier-Stokes equation for the flow problem. In this problem the assumption is made that the plates are infinitely wide and are very close to each other. For the solid equation, 5.2.2, the transient term and diffusive term are applied. The thermal conductivity is denoted by k, the density by ρ and the specific heat by c. All thermal and material properties are assumed constant except for the heat transfer, see chapter 3.

In order to properly assume adiabatic magnetization the magnetization will be done instantaneously. This way equation 2.2.17 can be used. The MCE will be formulated as a source term, which gives the following:

$$\frac{\delta T_s}{\delta t} = \frac{k_s}{\rho_s c_s} \left(\frac{\delta^2 T_s}{\delta x^2} + \frac{\delta^2 T_s}{\delta y^2} \right) + Q_{MCE} \quad (5.2.3)$$

Where Q_{MCE} is derived in chapter 2 and repeated here:

$$Q_{MCE} = -T \rho c_H \left(\frac{\delta M}{\delta T} \right)_H \frac{dH}{dt} \quad (5.2.4)$$

The hot heat exchanger is provided with a set temperature, independent from the systems performance. Other boundaries include thermal insulation and symmetry.

5.2.1 THE CONVECTIVE TERM

The energy equation, 5.2.1, contains the convective term, $-(u \cdot \nabla) T_f$, in which the fluid velocity is represented. This fluid flow is discretized by using the following analytical expression for the velocity field[8]:

$$u(y) = \bar{u} \left(\frac{6y^2}{H_f^2} - 1/2 \right) \quad (5.2.5)$$

This expression holds for steady, laminar fluid motion between to infinitely wide parallel plates. \bar{u} is the mean fluid velocity and H_f the height of the fluid channel.

5.2.2 INPUT PARAMETERS

In this subsection various parameters will be discussed and defined for further usage in later chapters.

TIMINGS

As described in the previous section four stages of the magneto refrigeration cycle can be identified. Every stages has a duration time of τ_x where $x = 1,2,3,4$. τ_1 and τ_3 represent the (de)magnetization timing and have the same value. τ_2 and τ_4 represent the fluid flow timings. The fluid flow timings will also be identical to each other. This creates a symmetrical timing pattern. However, this symmetrical timing pattern for the fluid flow could be favoured due to the changing heat capacity during (de)magnetization. Such asymmetrical timing is more difficult to imagine since it could induce an imbalance in the flow system: a net mass transport in positive or negative x-direction. However the asymmetrical timing is not considered further and of interest for future work.

A total cycle time can be denoted for one cycle: τ_{tot} and is given by $\tau_{tot} = \sum_{x=1}^4 \tau_x$

GEOMETRIC PARAMETERS

The regenerator can be geometrically defined using three variables: L_s length of the regenerator, H_s the thickness of the solid part and the thickness of the fluid channel, H_f . Now the porosity of the regenerator can be defined:

$$\epsilon = \frac{H_f}{(H_f + H_s)} \quad (5.2.6)$$

In order to determine the pressure drop across the regenerator the hydraulic diameter is required: defined as four times the flow cross section, divided by the wetted perimeter:

$$D_H = 2H_f \quad (5.2.7)$$

FLOW PARAMETERS

During τ_2 and τ_4 the flow is characterized by equation 5.2.5, the fluid inlet velocity, which is an input parameter. The fluid flow is modelled by two step functions, where the magnitude is determined by \tilde{u} . The second step function is in the opposite direction, creating an oscillatory flow.

Next to this the flow is characterized by the properties of the heat transfer fluid. The following relation is used to determine the length of a blow, or how far a fluid element is moved by average:

$$\delta x = \tilde{u}\tau_2 \quad (5.2.8)$$

For now it is relevant to consider the utilization factor, φ . This dimensionless parameter can be used to compare experimental results with numerical and is defined as the ration between the total thermal mass of the fluid moved and the thermal mass of the regenerator material:

$$\varphi = \frac{\dot{m}_f c_f \tau_2}{m_s c_s} \quad (5.2.9)$$

In case of a parallel plate situation this can be rewritten to:

$$\varphi = \frac{\rho_f c_f H_f \delta x}{\rho_s c_s H_s L_s} \quad (5.2.10)$$

$$(5.2.11)$$

The expression, 5.2.10, contains the heat capacity for the solid in the denominator. As discussed in chapter 3, this variable is strongly depended on temperature and magnetic field strength. As described in [31], the heat capacity used for a single material AMR is taken at T_C and 0T external magnetic field. When considering multiple materials a different approach is used: a weighted average would be more appropriate. The utilization factor and τ_2 are thus used to determine the \tilde{u} .

5.2.3 MESH AND TIME STEPPING

Due to the high non-linear behaviour of the magneto caloric effect numerical studies are justified. This in turn leads to the question what are the proper discretization dimensions. In order to obtain a reasonable temporal and spatial discretization an analytic attempt will be made in terms of the cooling capacity. In this case the regenerator will be simplified to have a single heat capacity and constant, albeit artificial, adiabatic temperature change. Assumed is a steady state condition and in this condition the magnetic work under no-load conditions should be equal to the amount of heat leaving the hot-side of the regenerator. The expression used for this condition is:

$$w_{mag} = c_s \rho_s (\Delta T_{ad,mag} + \Delta T_{ad,demag}) L_s H_s \quad (5.2.12)$$

In equation 5.2.12 L_s and H_s represent the dimensions: length and height of the regenerator. If c_s is chosen 235 $\text{Jkg}^{-1}\text{K}^{-1}$, which is a value representing the main heat capacity around the Curie temperature and letting $\Delta T_{ad,mag} = 4$ and $\Delta T_{ad,demag} = 3.5$ and set L_s and H_s 5 cm and 5 mm respectively. The result is $w_{mag} = 34.8 \text{ J m}^{-1}$.

To check whether the numerical set-up behaves as according to the quasi-analytical solution the geometrical dimensions are used as presented. Spatial and temporal resolutions influence the eventual magnitude of the adiabatic temperature difference and cooling capacity in a no load condition. Simulations will be performed reaching a steady state. A steady state is defined as two successive cycles have a lesser difference in terms of cooling capacity than the tolerance of the model (10^{-4}).

The mesh is deemed usable when the cooling capacity and adiabatic temperature change of the same experiment with changing spatial and temporal resolution are converged to a certain value. Next to this the analytical solution provides additional feedback about the quality of the discretization.

Table 5.2.1: Spatial and temporal resolution scheme.

Label	Spatial resolution (fluid, regenerator, HEX)	Timestep [s]
Ultra-Low	40x2, 20x2, 5x5	0.1
Low	80x5,40x5,5x5	0.05
Normal	160x10,80x10,10x10	0.01
High	320x20,160x10,20x20	0.001

Table 5.2.2: This table shows the model results. The normal resolution is seen to be sufficient for further studies using the model of the magnetocaloric effect.

Resolution	dt	$w_{max}[Jm^{-1}]$	$\Delta T_{noload}[K]$
Ultra low	0.5	0	0
Ultra low	0.1	27.5	6.95
Ultra low	0.01	34.3	8.46
Ultra low	0.001	34.2	8.28
Low	0.5	0	0
Low	0.1	27	7.30
Low	0.01	33.8	8.15
Low	0.001	34.5	8.26
Normal	0.05	33.5	8.23
Normal	0.01	34.3	8.51
Normal	0.001	34.5	8.29
High	0.005	34.5	8.30
High	0.001	34.5	8.31

The determined values are presented in table 5.2.2¹. It is concluded that the spatial and temporal resolution scheme *normal* can be used. The deviation in terms of cooling capacity determined by the numerical study from the analytical solution is 0.8%.

FOURIER NUMBER Another way of determining whether the spatial and temporal resolution are justified is by looking at the Fourier number. The Fourier number describes the relationship between the conductive transport rate to the quantity storage rate. This number can be used in order to analyse time dependent transport phenomena.

$$Fo = \frac{\alpha \cdot t}{L^2} \ll 1 \quad (5.2.13)$$

$$\alpha = \frac{k}{c_p \cdot \rho} \quad (5.2.14)$$

The main heat transport direction is in the y-direction for the solid domain and is therefore of main interest in this study. The velocity profile of the fluid is solved for in this study, therefore there is no need for a discretization of the velocity. For the different resolutions the Fourier number is on display in table 5.2.3. In all cases the Fourier criteria is met.

¹Table 5.2.2 is a summarized table of table .0.1 which can be found in the appendix .

Looking at the results in table 5.2.2* and 5.2.3 the use of the normal resolution is used. This holds a balance between computational time and accuracy. When using the normal setting the condition of a Fourier number as described in equation 5.2.13 is heavily met, this is due to the high transients in magnetization and fluid acceleration.

Table 5.2.3: Fourier numbers at different temporal and spatial resolutions.

Temporal / Spatial resolution	20x2	40x5	80x10	160x20
0.1(s)	0.012	0.0059	0.0030	0.0012
0.05(s)	0.0059	0.0030	0.0015	$5.91 \cdot 10^{-4}$
0.01(s)	$1.18 \cdot 10^{-5}$	$5.91 \cdot 10^{-5}$	$2.95 \cdot 10^{-5}$	$1.18 \cdot 10^{-4}$
0.001(s)	$1.18 \cdot 10^{-6}$	$5.91 \cdot 10^{-6}$	$2.95 \cdot 10^{-6}$	$1.18 \cdot 10^{-5}$

5.3 VALIDATION

The model is validated using the experiment as conducted by Paolo et. al. [29]. Paolo created a parallel plate AMR device, with reciprocating fluid flow and magnetic motion. Various parameters are copied and are listed in table 5.3.1. The distance between the most outer boundaries to the solid domain is chosen as 10mm. The outflow boundary condition is sensitive for the applied temperature as discussed. Therefore the distance between the solid and this boundary has to be large enough. The temperature of this boundary has to be influenced by the fluid. The effect of heat diffusion during the fluid stationary periods has to be minimized. Secondary effect of a longer length towards the AMR is the absence of entrance effects in the fluid. The simulation of this experiment is created by the means as discussed.

Table 5.3.1: This table contains the initial values and parameters of the numerical set-up to validate the numerical model. The model is validated by using the work of Paulo [29].

Variable	Value
L_s (mm)	160
d_s (mm)	0.85
H_f (mm)	0.1
$\tau_1 = \tau_3$ (s)	0.75
$\tau_2 = \tau_4$ (s)	1
Utilization(-)	0.2~0.8
H (A/m)	$8.0 \cdot 10^5$
T_{start} (K)	293

In order to determine the correct mass-flow the equation for the utilization factor is considered. However a deviating mass-flow is reported by Paolo et. al. This is probably due to experimental settings and flaws in making perfect channels. Therefore the reported mass-flow is used to determine the average velocity trough the channel in the model.

The magnetic field used in practice is modelled trough a term in the source term: $\frac{dH}{dt}$. This means that every part of the domain receives the exact same amount of magnetic field strength in the numerical experiment. According to Paolo this is not the case for the experimental set-up. In order to compensate for this effect the maximum magnetic field strength used in this design is 1 Tesla, the reported magnetic field strength by Paolo is around 1.22 Tesla.

The magnetic field is ramped up using the τ_1 as a transition time creating a (de)magnetization. Another important difference to notice is the presence of a magnetic field in the experimental set-up by Paolo. Looking at their set-up the MCM will never be totally free of a magnetic field. In the numerical model when no magnetic field is required, the magnetic field strength will be zero.

Concerning these two differences in terms of magnetic field behaviour throughout the thermodynamic cycle of the AMR the main goal of this validation is to determine whether the same behaviour in T_{ad} is observed. Primarily this means looking for an optimum value of T_{ad} at an utilization factor of 0.4 and secondarily looking for the same slope in the curve.

5.4 RESULTS

The model discussed so far was designed to simulate the behaviour of the active magnetic regenerative refrigeration magnetic cycle. Depending on the operating conditions, ie the change in utilization factor a steady state is achieved. The steady state is considered when the fluid temperature at the exit of the AMR in two successive cycles does not alter by more than 0.01K. Looking at the temperature plot of the exit, during the cycle the temperature varies therefore the temperature at the end of magnetization is taken as reference point.

During the steady state operation both extremities of the set-up have developed different temperatures and a temperature profile has been formed along the length of the regenerator due to the reciprocating flow.

In figure 5.4.1 we can observe the final temperature difference between the two extremities of the AMR for various utilization factors at a zero thermal load situation. The simulations were taken over approximately 250 seconds, depended on the cycle time, enough for a steady state to be achieved.

Looking at figure 5.4.1, the greatest temperature difference of 19.6 is achieved at a utilization factor of 0.4 which is in accordance to literature, [32],[29],[17]. And the smallest temperature difference found for this analysis is 16 for an utilization factor of 0.8.

For the studied utilization factors the temperature span developed smoothly following the typical profile line. This is interpreted as a properly functioning system where the fluid velocity is correlated with the frequency. When the utilization factor is above 0.5 the system is starting to move to fast and the fluid cannot extract all the heat properly from the solid. Next to this, due to the distance travelled by the fluid the regenerator is cooled to far during a hot blow and heated to high during a cold blow. The consequence is a lesser significant thermal gradient inside the regenerator which leads to a lesser increase in temperature difference between the two ends of the AMR.

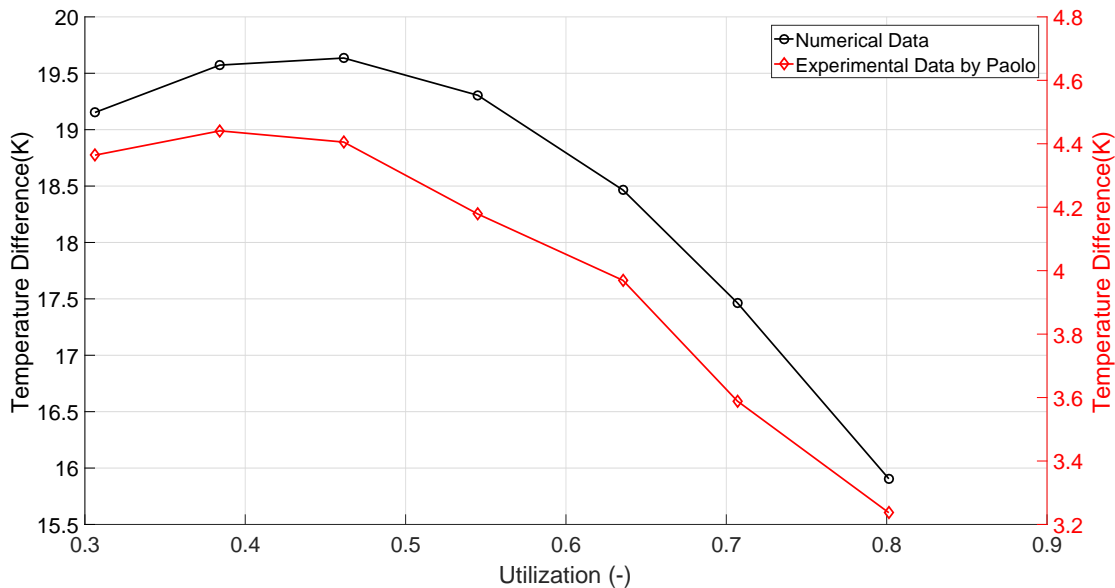


Figure 5.4.1: The no load temperature difference for both the numerical experiment as the laboratory experiment. Mind the right y-axis belonging to the experimentally obtained data.

5.5 DISCUSSION

Using the work from experimental, real life devices to validate models usually leads to difference in outcome. For this model this is also the case and primarily in the magnitude of the temperature difference. Various reasons can be found to explain the large difference in the values of the adiabatic temperature change. Next to this other experimental work can be considered to incorporate the difference in set-up.

Looking at the experimental set-up various important observations can be made. At first the device is finite and poorly thermal insulated. This means that the ambient air is in contact with the magneto caloric device heating up

the cold side, whereas the hot side is kept at a constant temperature. Due to this 'loss of cold' the final maximum temperature span is lower than expected in the numerical model. Insulation or the lack thereof is not taken into account in the model. The maximum temperature span is thus depended on the performance of the MCM and the maximum allowable temperature gradient by the thermodynamics.

The second observation is the use of commercially graded gadolinium. This material is observed and its (magnetic) characteristics are described in literature [7]. The numerical scheme uses material properties as calculated in chapter 3. Two distinctive differences can be made: first the material modelled is a perfect homogeneous material. Every part of the AMR has predictable magneto caloric properties. Whereas the experimental set-up is depended on forged gadolinium as can be found in nature. This influences its Curie temperature, T_C , whereas in the model the Curie temperature is fixed. Differences in Curie temperature could greatly affect the maximum attainable temperature span. The second difference is the representation of gadolinium by a model with its typical shortcomings.

In the numerical scheme the magnetic field is included in the magneto caloric effect via a direct method. The magnetic field term is modelled via the source term. Whereas in the experimental set-up the magnetic field is not exactly uniform. The uniformity of the magnetic field plays an important role in the performance of an AMR [30].

Lastly the numerical data can be compared to other experimental work. Data presented by Tusek et. al. in 2010 provides the same trend at higher temperatures. Their set-up managed to reduce heat losses to a minimum. Obtaining higher temperature differences between the two heat exchangers see figure 5.5.1.

It can be concluded that the model as described sufficiently predicts the behaviour of an AMR with gadolinium.

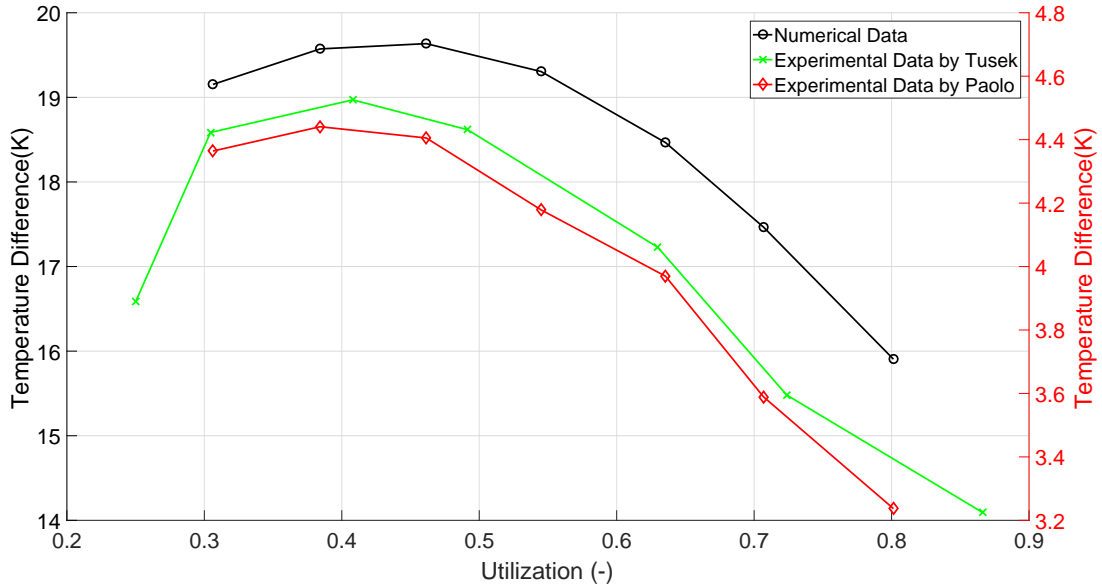


Figure 5.5.1: By looking at secondary experimental provided data the model can again be validated. The figure provides three plots(left y-axis): numerical, data provided by Tusek et. al. and data provided by Paolo (right y-axis).

2D MODEL - $Mn_{1.25}Fe_{0.7}P_{1-y}Si_y$ -AMR

The previous chapter describes the 2D model where gadolinium is used. A certain temperature span has been obtained. In order to increase this temperature span alternative materials could be investigated for the AMR. $Mn_{1.25}Fe_{0.7}P_{1-y}Si_y$ will be investigated in the current chapter.

6.1 INTRODUCTION

The previous chapter demonstrated the temperature difference that can be achieved using gadolinium. This can be used in practical applications: for example a refrigerator. However the ambient temperature has to be within the range of the T_C of gadolinium. Otherwise the performance of the MCE will drop in terms of cooling capacity and obtainable temperature span. In order to create an application that can operate in various ambient temperatures a more flexible set-up is required. This can be obtained by using various magneto caloric materials. These materials differ slightly in composition with the great advantage of only altering the T_C slightly, whilst other material properties remain fairly constant. The material family, as discussed in chapter 3, is $Mn_{1.25}Fe_{0.7}P_{1-y}Si_y$. This material has been developed by the material science group of prof.dr.ir. Brück from the Delft University and BASF material investigation.

Various observations are made by looking at the characteristics of the manganese family. Firstly the behaviour of this material is first order which means a narrow optimal MCE-performance band in terms of temperature. Taking advantage of the first order behaviour is nowadays normal practice to achieve large entropy and adiabatic temperature changes. This can be done by using the latent heat produced when the magnetic state changes.

The presence of latent heat has been discussed in chapter 3. In order to implement this latent heat production it is assumed that this is a reversible phenomenon. In order to model the latent heat the derivatives of the internal magnetization are slightly amplified. The result and comparison(with or without latent heat implementation) will be discussed later.

The second observation to be made is the large heat capacity variation throughout the magneto caloric cycle. It can be stated that the heat capacity behaves very asymmetrical in terms of the magneto caloric cycle. The result is that during the cold blow the MCM contains an high amount of thermal energy and during the hot blow the amount of thermal energy is much lower. During the cold blow the external magnetic field strength is high. The amount of mass required to cool the solid has to be high in comparison with the amount required to heat the solid again. However, the amount of fluid moved remains the same in both directions. In a refrigeration set-up this could lead to poor performance in terms of maximum temperature span at various utilization factors. The idea of different τ_2 and τ_4 comes to mind. This implies using a longer period to cool(hot blow) the solid, and a shorter(cold blow) to heat the solid. However, the result will be a net mass transport trough the domain which is impractical. In order to make use of these asymmetrical properties an attempt will be made to change the set-up: applying a cold heat source. A possible scenario for this set-up is the heating of a house with a cold heat source for example ground water. Other parameters will be unchanged. The expectation is that the temperature span over various utilization factors will be higher in comparison with the set-up using a hot heat source.

First the model that is created with Comsol Multiphysics has to be validated. This can be done by comparing the adiabatic temperature changes obtained trough the model with the direct measurements made by Brück [12].

6.2 EXPERIMENTS

This thesis is concerned with providing insight into the behaviour of $Mn_{1.25}Fe_{0.7}P_{1-y}Si_y$ as a MCM. In order to do this the experiment as described in chapter 5 is repeated. Various parameters are altered, the utilization being the most important. Next to this the overall length has increased to 240mm. The first series of experiments is conducted as previously described: a fixed hot heat exchanger and the cold heat exchanger as outflow boundary condition. A second series of experiments is conducted where the CHEX is kept a constant temperature of 275K. The HHEX is set as an outflow boundary condition: when the fluid has a negative direction, this boundary will provide the temperature as last received.

The domain is very similar to the domain of the gadolinium experiments of chapter 5. Some differences may be noted: the domain has been divided into four equal parts in geometry. Every part represents one of the four members of the $Mn_{1.25}Fe_{0.7}P_{1-y}Si_y$ family. From left to right the compound with $y = 0.49$ till $y = 0.52$ is placed. This can be explained by looking at the Curie temperature and the desired temperature span. Various dimensions and input parameters are listed in table 6.2.1. The numerical domain is represented in figure 6.2.1. The latest listed in the table is the temperature span. This span is deemed appropriate looking at the distribution of the Curie temperatures and the performance of the compounds as measured in literature.

Table 6.2.1: Input parameters $Mn_{1.25}Fe_{0.7}P_{1-y}Si_y$ experiment

Variable	Value
L_s (mm)	240
d_s (mm)	0.5
H_f (mm)	0.2
$\tau_1 = \tau_3$ (s)	0.75
$\tau_2 = \tau_4$ (s)	1
Utilization(-)	0.2~0.8
H (A/m)	$8.0 \cdot 10^5$
T_{start} (K)	[275 to 315]

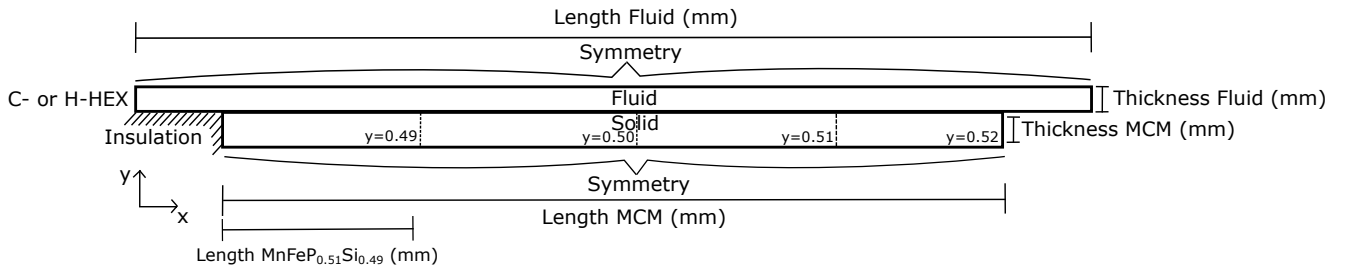


Figure 6.2.1: The solid domain has been split up into 4 even parts. However the length has increased into 4 times the original length of the gadolinium regenerator.

According to the literature the Curie temperatures of each part of the family is equidistant temperature wise. Therefore the solid can be divided into four parts of 60mm. The initial temperature gradient will be such that every compound is initially at its Curie temperature. This is illustrated in figure 6.2.2. The width of every box represents the geometrical width and the height of every box the maximum adiabatic temperature change above 1K for a magnetic field strength of approximately 1 Tesla. The various required material properties as discussed in chapter 3 will be used.

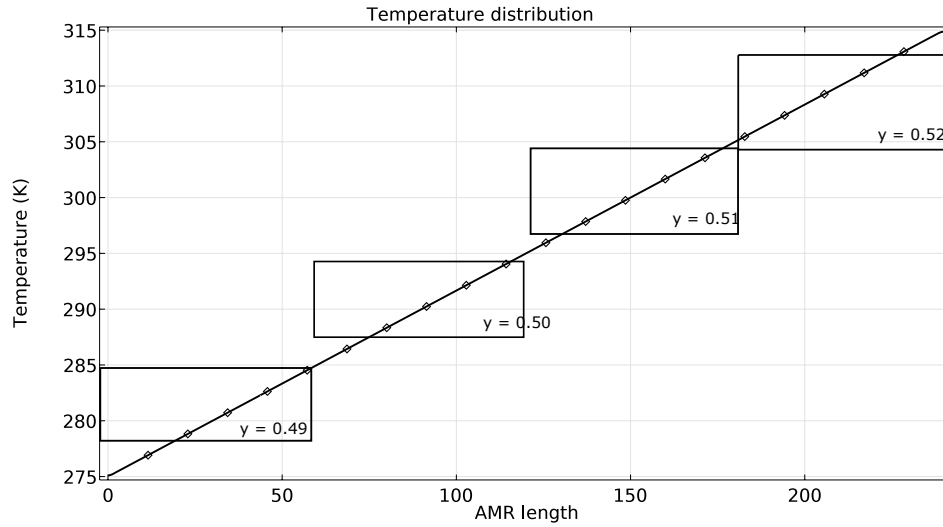


Figure 6.2.2: Initial temperature profile and distribution of the compounds in the domain. The height of the box represents the maximum adiabatic temperature change of that compound at 1 Tesla.

6.3 RESULTS

6.3.1 0D TEMPERATURE EXPERIMENTS

Various starting temperatures are considered, showing adiabatic temperature changes for each material respectively. Naturally the magnitude of this effect is depended on the derivative of the magnetization with respect to temperature, as discussed in chapter 3. The values(full line) found as displayed in figure 6.3.1 are in accordance with literature. It can be concluded that the first order magneto caloric effect is modelled sufficiently.

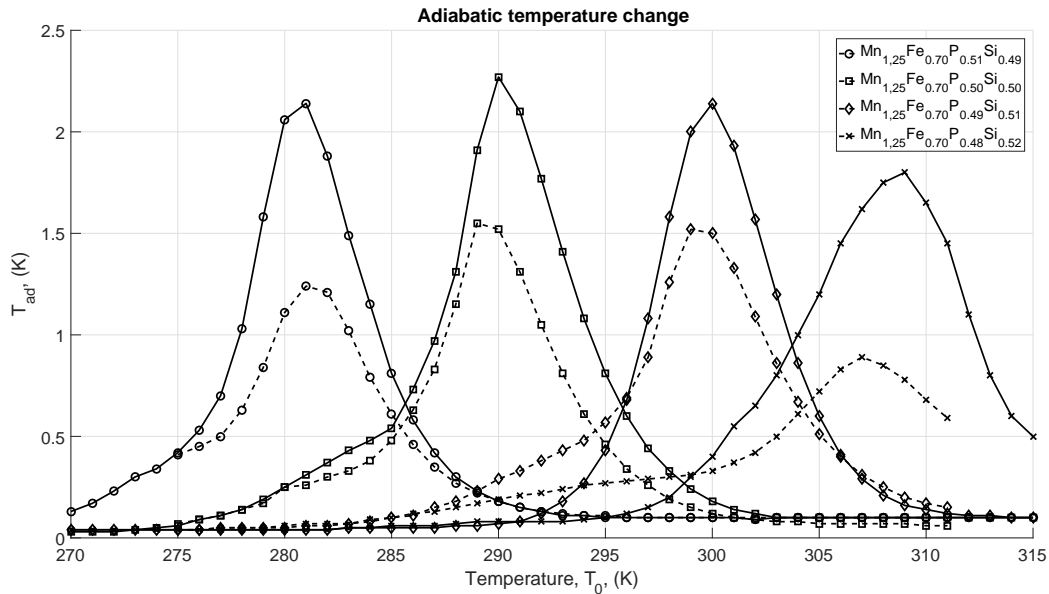


Figure 6.3.1: Adiabatic temperature change for the various compounds. The dashed lines represent the derived adiabatic temperature change excluding the latent heat.

6.3.2 2D UTILIZATION EXPERIMENTS

The utilization factor is an important parameter for the performance of the system. The utilization factor determines the distance a fluid package travels through the domain. This is important because of engineering aspects: if the utilization factor is low, the amount of fluid that leaves the AMR is too low to provide input for the heat exchanger.

The heat capacity plays an important role for determining a proper utilization factor. The heat capacity during the magnetization and (de) magnetization are presented in figure 6.3.2a and 6.3.2b. Looking at the distribution of the heat capacity over the AMR-length the four compounds of the $Mn_{1.25}Fe_{0.7}P_{1-y}Si_y$ family can be identified. During the cold blow period ($H = 1T$) it can be seen that the maximum values are $3600 J/(kg \cdot K)$ for $y=0.49$, $2950 J/(kg \cdot K)$ for $y=0.50$, $2590 J/(kg \cdot K)$ for $y=0.51$ and $600 J/(kg \cdot K)$ for $y=0.52$. During the hot blow period ($H = 0T$), the maxima are $600 J/(kg \cdot K)$ for $y = 0.49$, $550 J/(kg \cdot K)$ for $y = 0.50$, $560 J/(kg \cdot K)$ for $y = 0.51$ and $455 J/(kg \cdot K)$ for $y = 0.52$. It can be stated that there is a large difference in heat capacity for the both cases. Do mind that this difference is also due to the fact that the temperature gradient is as displayed in figure 6.2.2.

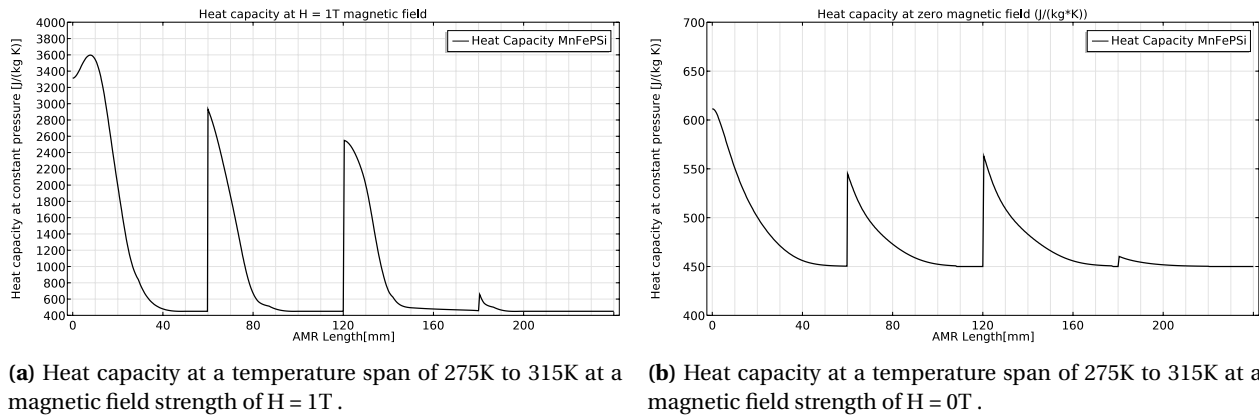


Figure 6.3.2: Heat capacity plotted against the length of the AMR.

At the beginning of each experiment a temperature gradient is applied. After magnetization, just previous of fluid flow, another temperature gradient can be measured. This is shown in figure 6.3.3. The green line represents the temperature after magnetization. Notice that the temperature did not rise equally throughout the domain.

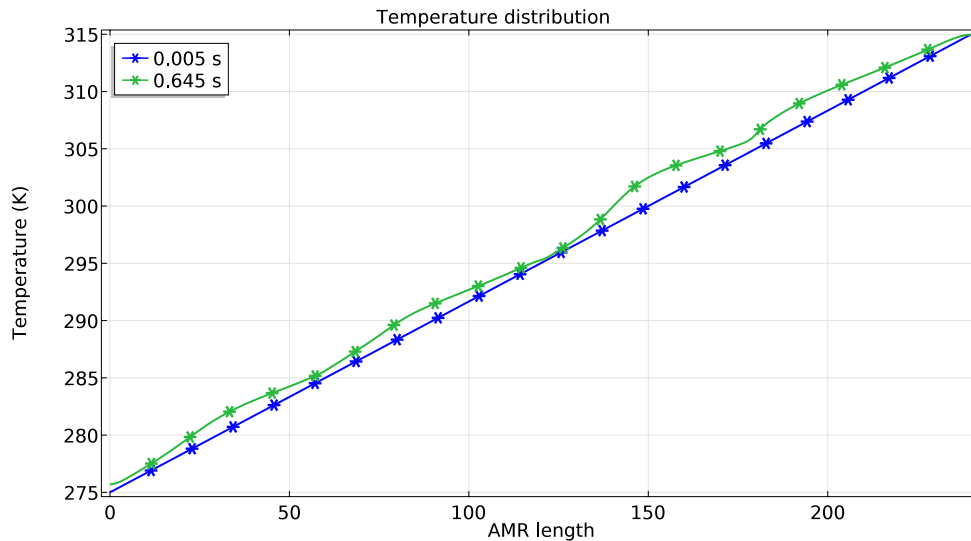
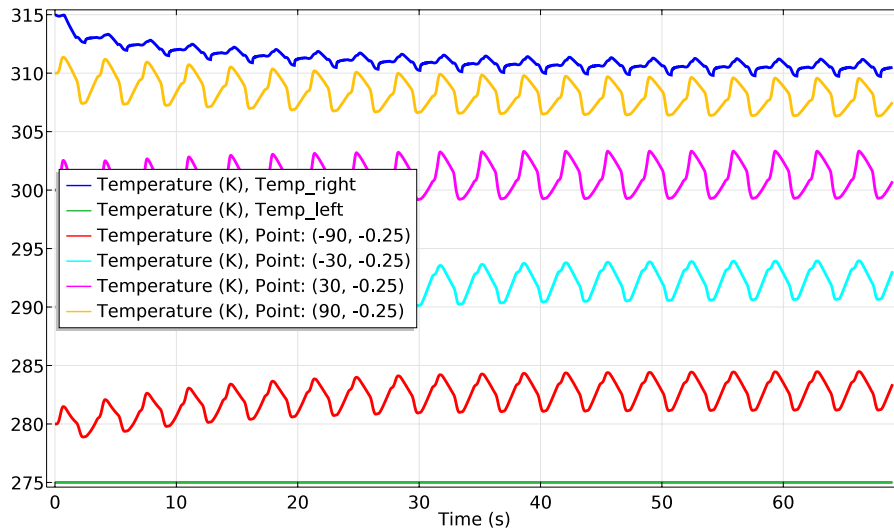


Figure 6.3.3: Temperature distribution before and after magnetization over the domain.

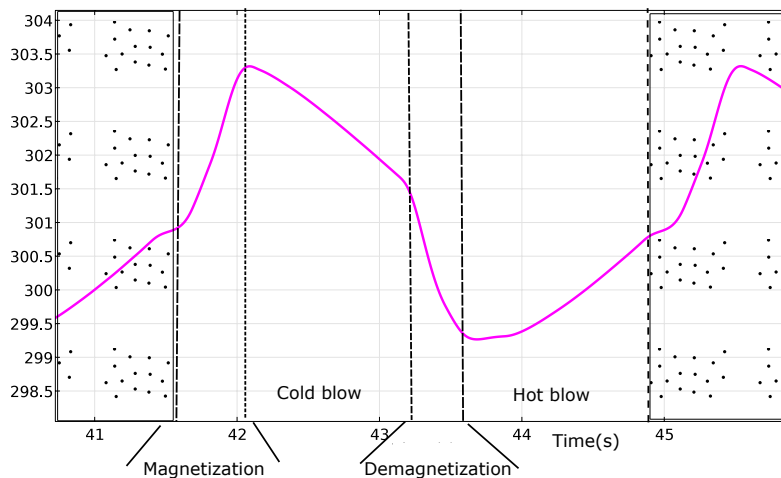
For every utilization factor a temperature gradient developed into a steady state. Meaning that the peak temperature during magnetization of two subsequent cycles differed less than 0.01K. The development of the temperature profile with utilization factor 0.1 is presented in figure 6.3.4a. This figure is taken from an experiment where the cold heat exchanger was kept at a constant temperature, whereas the hot heat exchanger was free. The four compounds are represented by colours: yellow ($y=0.52$), purple($y=0.51$), light blue ($y=0.50$) and red ($y=0.49$). The first three compounds tend to rise in average temperature during the first six cycle. The compound with $y=0.52$ lowers in temperature. After about 10 cycles a steady state has been reached.

In order to recognize the various stages of the thermodynamic cycle a close up of one of the compounds is presented in figure 6.3.4b. This figure shows the form of the temperature evolution in the regenerator. This cycle belongs to the $Mn_{1.25}Fe_{0.7}P_{1-y}Si_y$ with $y = 0.49$ compound. The four characteristic phases can be identified. This detailed figure is taken when a steady state was reached.

Looking back at figure 6.3.4a it can be noted that the compounds perform differently in temperature change due to (de) magnetization and fluid movements (cold and hot blow). The main reason for this variation is the distribution of heat capacity per compound.



(a) Temperature measured at various points in the domain. This plot is created with an utilization factor of 0.1



(b) Thermodynamic cycle for $Mn_{1.25}Fe_{0.7}P_{1-y}Si_y$ with $y = 0.49$, for an utilization factor of 0.1

Figure 6.3.4: Temperature development in the AMR.

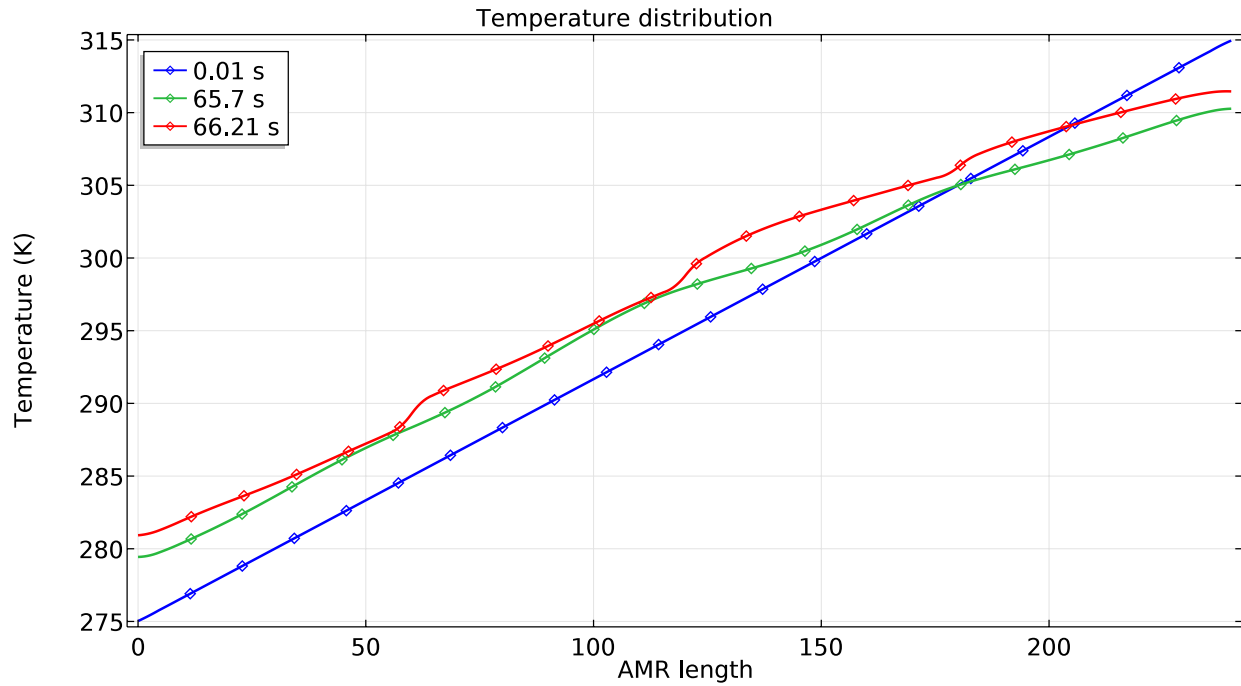


Figure 6.3.5: Temperature distribution before and after magnetization over the domain at steady state. The initial temperature distribution is also implemented to clarify the difference between initial and steady state.

Figure 6.3.5 displays the steady state temperature distribution (red and green line), the blue line displays the initial temperature distribution. The distribution has altered such that the Curie temperatures are not, more or less, in the middle of the domain. The plot is determined in the middle of the solid domain, therefore the temperature at zero AMR length is not 275K.

The utilization factor plays an important role in the determination of the fluid displacement. For this experiment the utilization factor is used, however the amount of fluid that was displayed is for this experiment the main variable. The fluid displacement is one of the key process parameters for an AMR [8]. In light of previous experiments the hot heat exchanger was kept at a constant temperature. The temperature difference between the hot and cold heat exchanger was determined at various utilization factors. This can be seen in figure 6.3.6. Next the cold heat exchanger was kept at a constant temperature: considering a heating setting. This can be seen that the heating setting performs better in terms of the temperature span. Both maxima are at the lowest utilization factor.

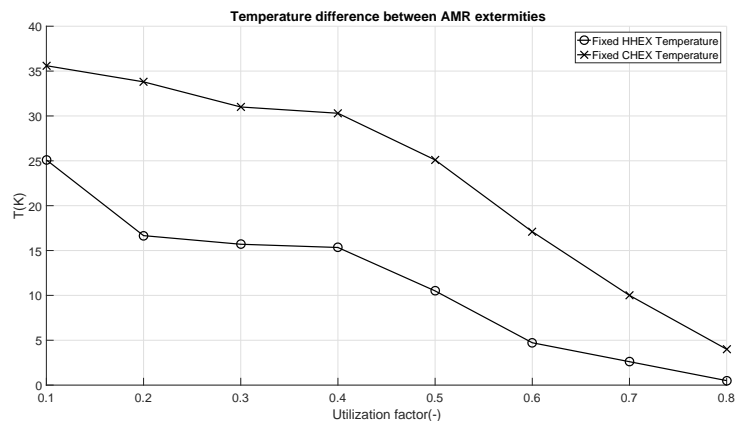


Figure 6.3.6: Temperature distribution before and after magnetization over the domain.

Lastly the comparison can be made between the manganese material family and gadolinium in terms of a no load temperature span. This can be seen in figure 6.3.7. A large difference is evident between the two materials in terms of a temperature span. This evidently proves the advantage of using materials with various Curie temperatures in series.

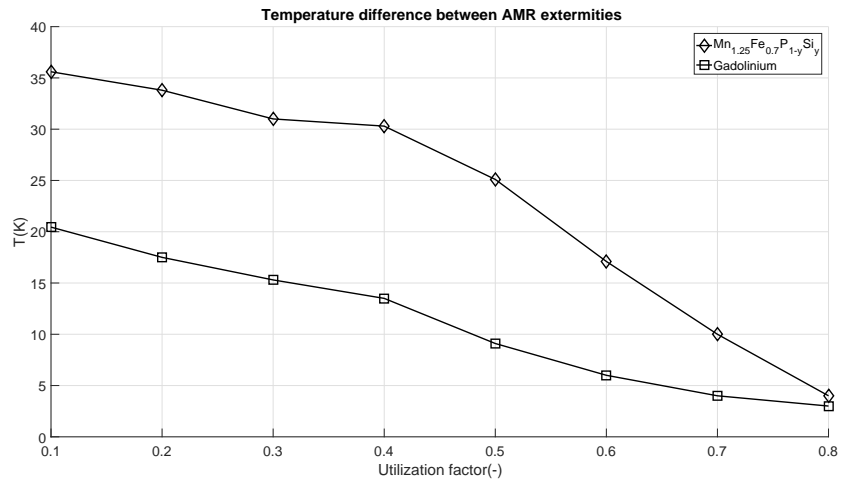


Figure 6.3.7: Temperature distribution before and after magnetization over the domain.

6.4 DISCUSSION

First thing to discuss is the saw-tooth profile of the heat capacity at high or low external applied magnetic fields, figure 6.3.2b and 6.3.2a. The heat capacity is purely depended on the temperature and applied magnetic field and are differently orientated per compound. The shape of both the adiabatic temperature and heat capacity are the roughly the same however, their peak values are at different temperatures (at the same magnetic field strength). For the compound where $y=0.52$, the far right in the domain has a larger difference between the two peaks temperature wise. This results in a smaller difference in heat capacity between the two magnetic states for temperatures around T_C .

The calculation of the utilization factor suffers greatly due to this large difference, or possibility of large difference in heat capacity when the local temperature was to change towards such a peak. The utilization factor has to be representative for both states, such that enough fluid is moved to alter the temperature gradient. In this experiment the utilization factor is kept constant. This means that for specific ranges of temperature gradients the utilization factor is sufficient.

The second thing to discuss is figure 6.2.2. The difference between $H=0T$ and $H=1T$ in temperature is made visible. The difference between the two lines can be seen as figure 3.6.1a. For this utilization factor this optimal temperature gradient remains fairly intact, however when the utilization factor increases the optimal gradient diminishes. And lower temperature differences are found.

Leading the discussion to figure 6.3.6. The first thing to notice is the large difference in temperatures between the two settings. In contrast to the fixed CHEX temperature the refrigerator setting performs poorly. Looking at figure 6.3.4a an explanation can be seen for this result: during the hot blow, moving fluid from the hot side, the material is easily heated up. This is mostly visible during the early cycles. The utilization factor for this part of the cycle is overestimated: the heat capacity is taken to high with a too large fluid displacement as a consequence. The high heat capacity seems to work as a diode for heat when configured with a fixed cold heat exchanger temperature. The heat capacity is high during magnetization, and a positive fluid flow. During this cold blow very little heat is being taken up by the fluid in comparison to the heat being absorbed by the MCM during the hot-blow. Leaving a system which heats up more easily. Adding the MCE to this, which happens before the cold blow, the system is apparently prone to be more effective in a as a heating system.

The compound closest to the fixed temperature heat exchanger can use this as a heat source whereas the other compounds rely on neighbouring parts to provide for the heat sink or source function. Due to an increasing utilization factor the fluid displacement distance increases as well. This means that heat can travel further than the part its meant to go to. The heat transfer is insufficient to alter the thermal energy content of the fluid. The consequence is the movement of heat to parts of the regenerator. This in turn leads to a temperature alteration that does not suit the particular compounds Curie temperature. Proper functioning of this part is lost. As can be seen in table 6.4.1 at an utilization factor of 0.4 the fluid displacement surpasses the length of an compound ($L_{\text{compound}} = 60\text{mm}$).

Table 6.4.1: The fluid displacement distances at the used utilization factors.

Utilization factor(-)	0.1	0.2	0.4	0.6	0.8
Fluid displacement(mm)	17	35	71	107	142

CONCLUSION AND DISCUSSION

This is the final chapter summarizing the conclusions found the the previous chapter. Next to this several recommendation are made as suggestion for further investigation.

7.1 0D MODEL

Previous work at the Twente University showed inconsistencies in the energy balance of the magnetocaloric effect. A 0D model was created to investigate. Three main contributions to the energy equation were identified and modelled. According to the energy equation these energies should add up to zero, which it does. It can be concluded that the first law is obeyed by the system as described. The relative error is mainly depended on the numerical scheme. In order to obtain an scientific accepted error a time step of 10^{-4} is required. Using this time step the sum of energies is nearing zero. Next to this the initial temperature after the magneto caloric cycle is reached again. This implies that there is no residual energy left.

7.2 2D MODEL - GADOLINIUM

The second part of the thesis was to develop a 2D model of an AMR. For this model gadolinium was used as the magneto caloric material. The properties of this material are described by the mean field theory. Gadolinium is a common material in the magnetocaloric effect research as a refrigerator. Numerical and experimental data are available to validate the model.

A mesh and validation study are performed. The mesh study provided temporal and spatial settings to use for the validation study. The validation study concerns measuring the temperature difference between the two heat exchangers after a steady state is reached. This is done for various utilization factors. The model is deemed validated albeit that the temperatures found differ from literature: the trend is the same and the magnitude differences can be accounted for.

7.3 2D MODEL - $Mn_{1.25}Fe_{0.7}P_{1-y}Si_y$

The model as described in chapter 5 was adapted to accommodate the $Mn_{1.25}Fe_{0.7}P_{1-y}Si_y$ material family. The model proved to reproduce the adiabatic temperature changes for every member of the family in accordance with literature. Two studies have been conducted: both the CHEX as the HHEX have been kept at constant temperatures. The temperature difference between the two were registered as function of the utilization factor. The initial temperature span for every simulation was kept the same. The results showed large differences between the two settings. In the heating configuration the largest temperature span was obtained. The primary reason for the large difference is the heat capacity distribution. In comparison with gadolinium in the heating setting the use of materials with different Curie temperatures proves to achieve a larger temperature span.

7.3.1 RECOMMENDATION: 2.5D MODEL

For both experiments (for gadolinium and $\text{Mn}_{1.25}\text{Fe}_{0.7}\text{P}_{1-y}\text{Si}_y$) an ideal situation was assumed: no heat losses were modelled or taken into account. However to predict the systems performance more accurate a heat loss model should be implemented. For the gadolinium AMR 2.5D models are presented and validated through experimental research. Such heat loss models should be implemented into the $\text{Mn}_{1.25}\text{Fe}_{0.7}\text{P}_{1-y}\text{Si}_y$ AMR model as well. This will provide a more accurate prediction of the performance. The overall goal of this model is to gain insight in the behaviour of $\text{Mn}_{1.25}\text{Fe}_{0.7}\text{P}_{1-y}\text{Si}_y$ as a MCM. Further more the material is difficult to create and its main production process depends on sintering. One of the major problems is to manufacture these in to fine and porous geometries for an efficient heat transfer [30]. The used heat transfer coefficient is calculated based upon the composition of the compounds. However, the structure of the material has not been taken into account. For thin plates as used in this numerical model the influence is not too large.

7.3.2 RECOMMENDATION: UTILIZATION FACTOR

In order to keep comparing experiments with each other it is necessary to keep utilization factors constant. However, as can be concluded from these experiments this is not sufficient. Therefore, by making use of the fact it is a dimensionless number, various parameters in equation 5.2.10 could be altered in such a way that the outcome remains the same, but changing the fluid displacement distance. In order to do this an changing average of the heat capacity is in place. As stated before the net mass transport has to remain zero, implying that the fluid displacement distance over a total cycle has to remain zero.

The utilization factor has also practical engineering aspects to it: using low utilisation factors means also very little fluid is moved out of the AMR. Looking at the primary experiment concerning $\text{Mn}_{1.25}\text{Fe}_{0.7}\text{P}_{1-y}\text{Si}_y$ the utilization factor was varied from 0.1 to 0.8. However, due to the long domain at the lower utilization factors could be used due to have a significant wash-out of cold or hot fluid for the heat exchanger.

The engineering problem of low utilization factor is the amount of fluid that is being pumped in and out of the system: there is little fluid to interact with in the heat exchangers at the extremities of the system.

BIBLIOGRAPHY

- [1] V. Gschneidner, K., Pecharsky. Thirty years of near room temperature magnetic cooling: where we are today and future prospects. *International Journal of Refrigeration*, 34:945–961, 2008.
- [2] Pecharsky V K Gschneidner K A and Tsokol A O. No Title. *Rep. Prog. Phys.*, 2005.
- [3] Nielsen K K Smith A, Bahl C R H, Bjørk R, Engelbrecht K and And Pryds. No Title. *Adv. Energy Mater.*, 2:1288, 2012.
- [4] M. Isaac Vuuren and D. P. Van. Modeling global residential sector energy demand for heating and air conditioning in the context of climate change. *Energy policy*, 37:507–521, 2009.
- [5] W. Goetzler, R. Zogg, J. Young and C. Johnson. Energy savings potential and rd&d opportunities for non-vapor-compression hvac technologies. *Navigant Consulting Inc., prepared for US Department of Energy*, 2014.
- [6] Andrej Kitanovski, Jaka Tušek, Urban Tomc, Uroš Plaznik, Marko Ožbolt, and Alojz Poredoš. *Magnetocaloric Energy Conversion*, volume 179. 2015.
- [7] S. Dan'kov, a. Tishin, V. Pecharsky, and K. Gschneidner. Magnetic phase transitions and the magnetothermal properties of gadolinium. *Physical Review B*, 57(6):3478–3490, 1998.
- [8] K.K. K. Nielsen, C.R.H. R H Bahl, A. Smith, R. Bjørk, N. Pryds, and J. Hattel. Detailed numerical modeling of a linear parallel-plate Active Magnetic Regenerator. *International Journal of Refrigeration*, 32(6):1478–1486, 2009.
- [9] K. Engelbrecht and C. R H Bahl. Evaluating the effect of magnetocaloric properties on magnetic refrigeration performance. *Journal of Applied Physics*, 108(12), 2010.
- [10] A. Rowe. Configuration and performance analysis of magnetic refrigerators. *International Journal of Refrigeration*, 34(1):168–177, 2011.
- [11] K. Engelbrecht, C. R H Bahl, and K. K. Nielsen. Experimental results for a magnetic refrigerator using three different types of magnetocaloric material regenerators. *International Journal of Refrigeration*, 34(4):1132–1140, 2011.
- [12] H Yibole, F Guillou, L Zhang, N H van Dijk, and E Brück. Direct measurement of the magnetocaloric effect in MnFe(P, <i>X</i>)(<i>X</i> = As, Ge, Si) materials. *Journal of Physics D: Applied Physics*, 47(7):075002, 2014.
- [13] A. Pecharsky, V., Gschneidner, K., Pecharsky, A., and Tishin. Thermodynamics of the magnetocaloric effect. *Physical Review B (Condensed Matter and Materials Physics)*, 64(144406):1–13, 2001.
- [14] W. F. Giauque and D. P. MacDougall. Attainment of Temperatures Below 1Å Absolute by Demagnetization of Gd₂(SO₄)₃·8H₂O. *Physical Review*, 43(9):768–768, 1933.
- [15] G. V. Brown. Magnetic heat pumping near room temperature. *Journal of Applied Physics*, 47:3673–3680, 1976.
- [16] C Kittel. Introduction to solid state physics. *John Wiley & Sons, Inc.*, New York,, 1996.
- [17] K.K. Nielsen, C.R.H. Bahl, A. Smith, N. Pryds, and J. Hattel. A comprehensive parameter study of an active magnetic regenerator using a 2D numerical model. *International Journal of Refrigeration*, 33(4):753–764, 2010.

- [18] Kaspar Kirstein Nielsen, Jesper Henri Hattel, Nini Pryds, Christian Robert Haffenden Bahl, and Anders Smith. *Numerical modeling and analysis of the active magnetic regenerator*. PhD thesis, 2010.
- [19] Morrish, A.H. *The Physical Principles of Magnetism*. John Wiley & Sons, Inc., 1965.
- [20] D. Ashcroft, N. W. and Mermin. *Solid State Physics*. Saunders College, 1976.
- [21] D. Lide. *CRC Handbook of Chemistry and Physics*. CRC Press, 2004.
- [22] Y. Tishin, A. and Spichkin. *The Magnetocaloric Effect and its Applications*. Institute of Physics Publishing, 2003.
- [23] A. Rowe and A. Tura. Experimental investigation of a three-material layered active magnetic regenerator. *International Journal of Refrigeration*, 29(8):1286–1293, 2006.
- [24] Michael G. Schroeder and Ellen Brehob. A flexible numerical model of a multistage active magnetocaloric regenerator. *International Journal of Refrigeration*, 65:250–257, 2016.
- [25] Jaka Tušek, Andrej Kitanovski, Urban Tomc, Chiara Favero, and Alojz Poredoš. Experimental comparison of multi-layered La-Fe-Co-Si and single-layered Gd active magnetic regenerators for use in a room-temperature magnetic refrigerator. In *International Journal of Refrigeration*, volume 37, 2014.
- [26] W De Vries. APPLICATION OF PELTIER THERMAL DIODES IN A MAGNETOCALORIC HEAT PUMP. 2016.
- [27] J. Stöter. *MODELING OF A MAGNETOCALORIC HEAT PUMP IN COMSOL*. 2016.
- [28] Jaka Tušek, Andrej Kitanovski, Samo Zupan, Ivan Prebil, and Alojz Poredoš. A comprehensive experimental analysis of gadolinium active magnetic regenerators. *Applied Thermal Engineering*, 53(1):57–66, 2013.
- [29] Paulo V. Trevizoli, Jader R. Barbosa, and Rogério T S Ferreira. Experimental evaluation of a Gd-based linear reciprocating active magnetic regenerator test apparatus. *International Journal of Refrigeration*, 34(6):1518–1526, 2011.
- [30] Jaka Tušek, Andrej Kitanovski, and Alojz Poredoš. Geometrical optimization of packed-bed and parallel-plate active magnetic regenerators. *International Journal of Refrigeration*, 36(5):1456–1464, 2013.
- [31] A. Tura, A. and Rowe. Progress in the characterization and optimization of a permanent magnet magnetic refrigerator. *Third International Conference on Magnetic Refrigeration at Room Temperature*, pages 387–392, 2009.
- [32] Sergiu Lionte, Carmen Vasile, and Monica Siroux. Numerical analysis of a reciprocating active magnetic regenerator. *Applied Thermal Engineering*, 75:871–879, 2015.

NOMENCLATURE

ACRONYMS

AMR	Active Magnetic Regenerator
MCE	Magneto Caloric Effect
MCM	Magneto Caloric Material
MFT	Mean Field Theory

ROMAN SYMBOLS

c	specific heat capacity	$[Jkg^{-1}K^{-1}]$
d	thickness	$[mm]$
Fo	Fourier number	$[-]$
k	thermal conductivity	$[WK^{-1}]$
L	length	$[mm]$
\dot{m}	mass flow	$[kgs^{-1}]$
t	time	$[s]$
T	temperature	$[K]$
H	height	$[mm]$
D_H	hydraulic diameter	$[mm]$
u	velocity	$[ms^{-1}]$
\bar{u}	average velocity	$[ms^{-1}]$
y	height of channel	$[mm]$
M	magnetization	$[Am^2kg^{-1}]$
H	applied magnetic field	$[Am^{-1}]$
S	entropy	$[JK^{-1}]$
q	specific heat	$[Jkg^{-1}K^{-1}]$
g	Lande factor	$[-]$
J	Total angular momentum	$[J(h)]$
k_b	Boltzman constant	$[JK^{-1}]$
N_s	Number of magnetic spins	$[kg^{-1}]$

GREEK SYMBOLS

μ	magnetic permeability	$[TmA^{-1}]$
ρ	density	$[kgm^3]$
Θ_D	Debye temperature	$[K]$
γ	Sommerfeld constant	$[Jkg^{-1}K^{-2}]$
μ_B	Bohr magneton	$[JT^{-1}]$
τ_i	period	$[s]$
ϵ	porosity	$[-]$
φ	Utilization factor	$[-]$
α	Thermal conductivity	$[Wm^{-1}K^{-1}]$

0D MODEL FIGURES

In order to ensure readability in chapter 4, several figures are left out and presented here. These figures provide a more detailed insight in each contribution of the parts of the total internal energy balance. In figure the non-cumulative heat source is presented. This differs from the energy figure in chapter 4. The last figure shows the internal magnetization of the material. Interesting to see how this changes in accordance to the magnetization prediction by the mean field theory.

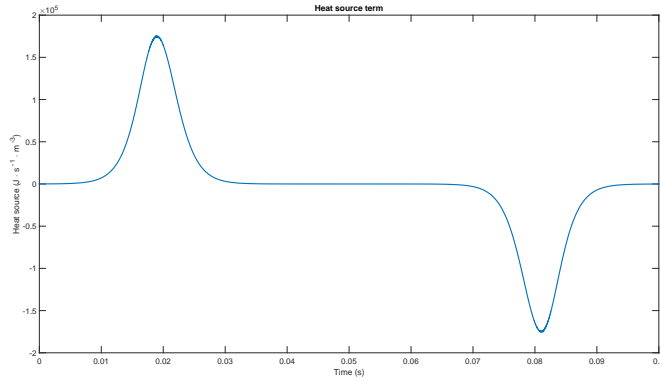


Figure .0.1: The \dot{Q}_{MCE} is presented here.

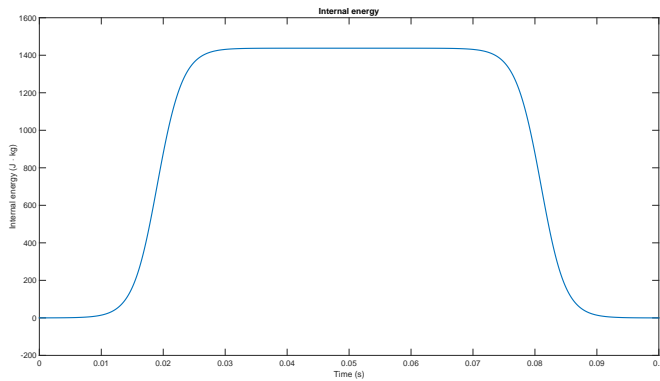


Figure .0.2: The internal energy is presented here.

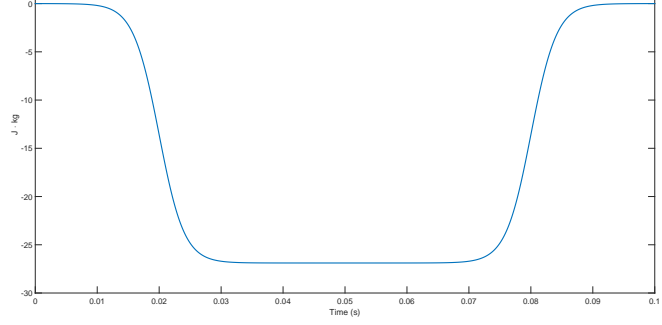


Figure .0.3: The magnetic work is presented here.

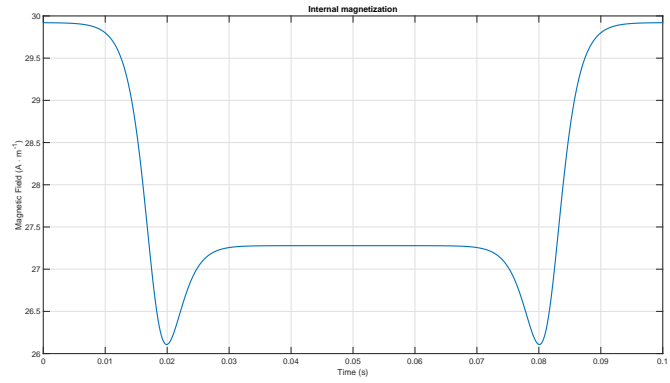


Figure .0.4: The internal magnetic field is presented here.

FULL RESULTS 2D MODEL

The table shows the all the results obtained by the first validation study of the 2D model using gadolinium. In the main matter a shortened version is presented for readability purposes.

Table .0.1: Full results of the mesh study

Resolution	dt	$w_{max}[Jm^{-1}]$	$\Delta T_{noload}[K]$
Ultra low	0.5	0	0
Ultra low	0.1	27.5	6.95
Ultra low	0.05	32	7.05
Ultra low	0.01	34.3	8.46
Ultra low	0.005	34.3	8.32
Ultra low	0.001	34.2	8.28
Low	0.5	0	0
Low	0.1	27	7.30
Low	0.05	30	8.16
Low	0.01	33.8	8.15
Low	0.005	34.5	8.28
Low	0.001	34.5	8.26
Normal	0.5	0	0
Normal	0.1	27.5	6.92
Normal	0.05	33.5	8.23
Normal	0.01	34.3	8.51
Normal	0.005	34.3	8.31
Normal	0.001	34.5	8.29
High	0.1	28	6.87
High	0.05	31.5	7.32
High	0.01	34.4	8.51
High	0.005	34.5	8.30
High	0.001	34.5	8.31